# Perfusion Imaging Using Arterial Spin Labeling

*Xavier Golay, PhD,* Jeroen Hendrikse, MD,† and Tchoyoson C. C. Lim, MD**

**Abstract:** Arterial spin labeling is a magnetic resonance method for the measurement of cerebral blood flow. In its simplest form, the perfusion contrast in the images gathered by this technique comes from the subtraction of two successively acquired images: one with, and one without, proximal labeling of arterial water spins after a small delay time. Over the last decade, the method has moved from the experimental laboratory to the clinical environment. Furthermore, numerous improvements, ranging from new pulse sequence implementations to extensive theoretical studies, have broadened its reach and extended its potential applications. In this review, the multiple facets of this powerful yet difficult technique are discussed. Different implementations are compared, the theoretical background is summarized, and potential applications of various implementations in research as well as in the daily clinical routine are proposed. Finally, a summary of the new developments and emerging techniques in this field is provided.

**Key Words:** perfusion imaging, arterial spin labeling, spin tagging, cerebral blood flow, quantitative MR imaging

(*Top Magn Reson Imaging* 2004;15:10–27)

## ARTERIAL SPIN LABELING: THE BASICS

Arterial spin labeling (ASL) is based on the principles of the indicator dilution theory. This theory was used for the first time by Kety and Schmidt to measure cerebral blood flow (CBF) in humans.[1,2] Their method was based on the measurement of the arteriovenous dynamics of a freely diffusible tracer, nitrous oxide ($N_2O$), passed into the arterial system through the respiration. Since the concentration of arterial tracer, $c_a(t)$ increases faster that the venous concentration $c_v(t)$, the regional CBF can be estimated using Fick's principle:

$$\frac{dC_T(t)}{dt} = CBF(c_a(t) - c_v(t)) \qquad (1)$$

with $C_T(t)$ the tissue concentration of the tracer. In this model, the venous concentration of the tracer is corrected for the difference in blood and tissue water contents: $C_v(t) = C_T(t)/\lambda$ with $\lambda$ = blood–brain partition coefficient, which can be different for different tissues.[3]

While the Kety-Schmidt method is rarely used in patients today, their theory has been applied for the estimation of rCBF in numerous techniques, mainly using radioactive tracers, such as $H_2{}^{15}O$ in positron emission tomography (PET)[4,5] or $^{99m}$Tc-ethylcysteinate-dimer in single-photon emission computed tomography.[6] Similar methods using intra-arterial injection of non-$^1$H NMR-visible tracers have been proposed using Kety-Schmidt's quantification theory. For recent review articles of the MR methodologies to measure perfusion, see Barbier et al,[7] Calamante et al,[8] or the book chapter by Alsop.[9]

In ASL, no extrinsic tracer is used. Instead, a selective preparation sequence is applied to the arterial water spins, and the perfusion contrast is given by the difference in magnetization or apparent relaxation time induced by the exchange of these labeled spins with the tissue of interest[10–12] (Fig. 1).

The original ASL method for labeling arterial spins was proposed by Williams et al.[13] In this work, the authors used a single volume coil at the level of the common carotid arteries to invert the spin adiabatically in a way similar to an earlier published angiography technique.[14] The degree of labeling of this ASL method is highly dependent on the adiabatic labeling condition[13,15–17]:

$$1/T_1, 1/T_2 << G \cdot v/B_1 << \gamma B_1 \qquad (2)$$

with $T_1$, $T_2$ the spin-lattice and spin-spin relaxation times respectively (in s), $G$ = gradient strength (in mT/m), $v$ = the normal nominal mean blood velocity in the vessels, $\gamma$ = gyromagnetic moment ratio for $^1$H and $B_1$ is the amplitude (in mT) of the applied RF amplitude. Typical values for the degree of inversion achieved with such method vary between 80% and 90%, depending on the choice of $G$ and $B_1$.[15,16,18] While continuous adiabatic inversion is still used today to measure perfusion, new sequences appeared soon after, in which the magnetic labeling of the spins is performed at once over a wide spatial range to get better inversion efficiencies.[10,19,20] These methods are referred to as pulsed arterial spin labeling (PASL) as opposed to continuous arterial spin labeling (CASL) for the original scheme using flow-driven adiabatic inversion of the arterial spins.

From the *Department of Neuroradiology, National Neuroscience Institute, Singapore; and the †Department of Radiology, University Medical Center, Utrecht, The Netherlands.

Address correspondence and reprint requests to Xavier Golay, PhD, Department of Neuroradiology, National Neuroscience Institute, 11 Jalan Tan Tock Seng, Singapore, 308433 (e-mail: Xavier_Golay@ttsh.com.sg).

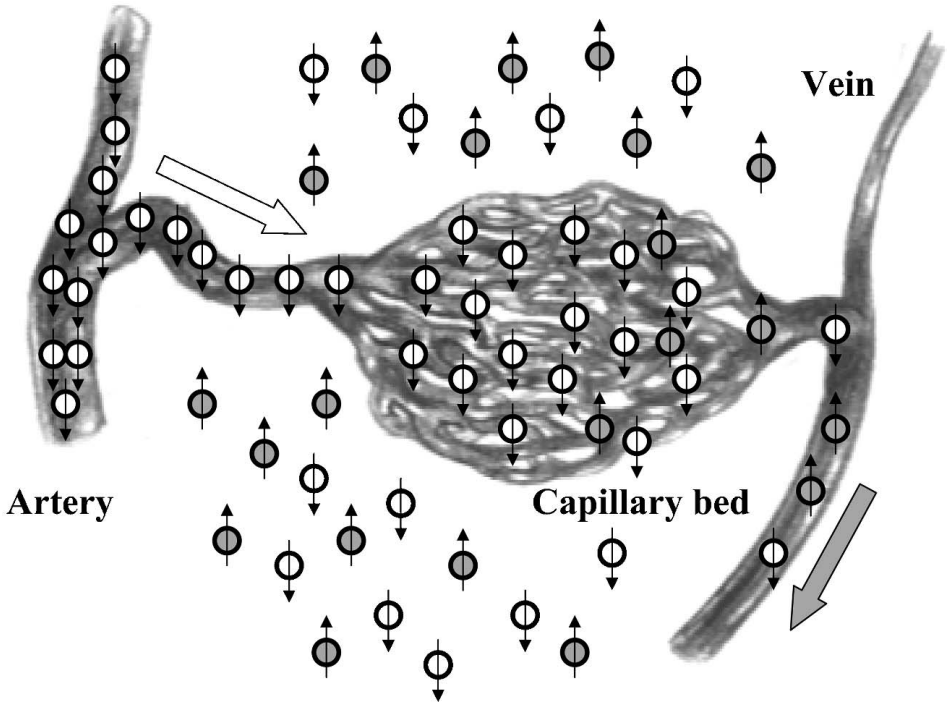


**FIGURE 1.** Schematic description of the principles of freely diffusible tracer theory. Inverted magnetization (white) comes from the arterial tree (white arrow) and diffuses through the blood–brain barrier at the capillary level. There, spins are exchanged with the tissue magnetization (gray), and reduce its local intensity. The degree of attenuation is a direct measure of perfusion. Remaining tagged magnetization as well as exchanged water molecules flow out of the voxel of interest through the venous system (gray arrow).

Indeed, it was the development of PASL techniques that moved the whole field from laboratory animals to the humans.[11] The successful application of such methods to noninvasively determine brain perfusion imaging in humans attracted a larger number of people to work in this field, and the number of scientific or clinical papers yearly published on this topic exploded from a few papers published yearly until 1996 to over 20 from the year 1999 onwards (Fig. 2).

## MR TECHNIQUES FOR ASL

### Continuous Arterial Spin Labeling (CASL) Techniques

The very first implementation of ASL was done using long RF pulses in combination with a slice-selection gradient to adiabatically invert the arterial magnetization.[11,13,15] It was immediately recognized that a potential confounding factor of this method is that it induces magnetization transfer (MT) effects.[21] Indeed, the application of long off-resonance RF pulses will induce a saturation of the backbone of large macromolecules in the tissue included in the imaging coil, due to their broad resonance frequencies.[22] Once saturated, this large macromolecular pool will then exchange its magnetization with that of the "free" water, inducing in that way changes in both $T_1$ relaxation time and magnetization similar to those produce by ASL and therefore leading to an overestimation of the perfusion effects.[11] To overcome this problem, a distal labeling of the magnetization is performed in the control experiment to produce identical MT effects. This method works well for single-slice perfusion imaging; however, the long RF pulses used in such techniques are applied concurrently with a gradient pulse and therefore render MT effects dependent on the slice position.

Other techniques are necessary to control for these effects in a global way. The simplest one is to use a second coil to perform the adiabatic continuous inversion.[23,24] In such a situation, the RF saturation pulse does not affect the tissue of interest due to the localized $B_1$ field of the second labeling coil. The use of both separate gradient and RF coils for ASL has also been proposed and would be more useful for human brain perfusion imaging in head-only scanners, or other systems with restricted gradient coils.[25] Furthermore, the use of additional coil for labeling has the added feature of being able to selectively label the left or right common carotid artery independently, therefore allowing some kind of perfusion territory mapping.[26,27]

Another possibility, as originally proposed by Alsop and Detre, is to control globally for MT effects using a sinusoidal modulation of the RF waveform.[28] The application of such an RF pulse together with a gradient will continuously saturate two planes at the same time, resulting theoretically in a net zero labeling during the control phase. The RF power is adjusted so that the root mean square power is identical in both labeling and control acquisitions to produce identical MT effects. The main drawback of this method is that imperfections in the double-inversion plane usually result in a lower labeling efficiency (~70%).[28] An example of an image acquired with this

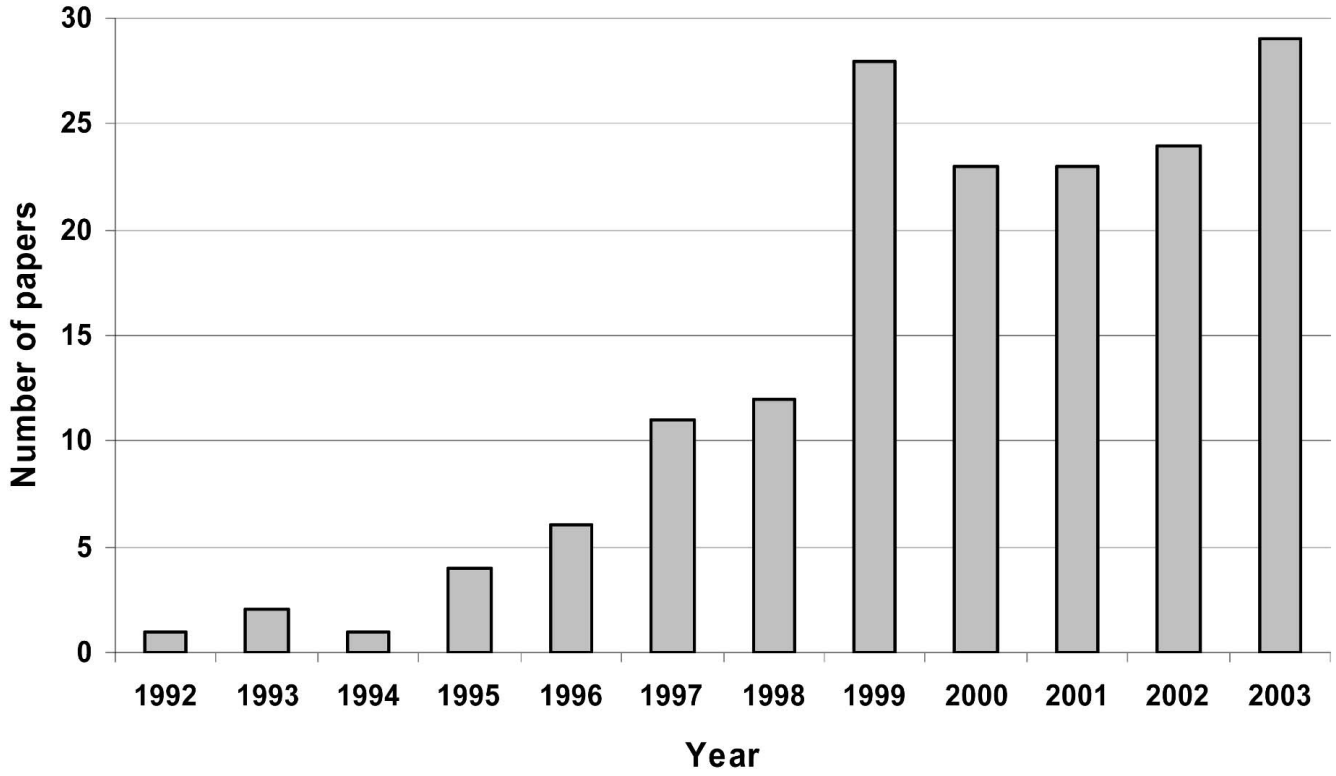


**FIGURE 2.** Bar plot of the number of papers provided by a simple Medline search using "Arterial Spin Labeling" or "Arterial Spin Tagging" as key words.

technique is shown in Figure 3, in which three slices (out of 15 acquired) are shown for both a healthy 10-year-old girl and a female patient suffering from Rett syndrome, a rare neurogenetic disease.[29]

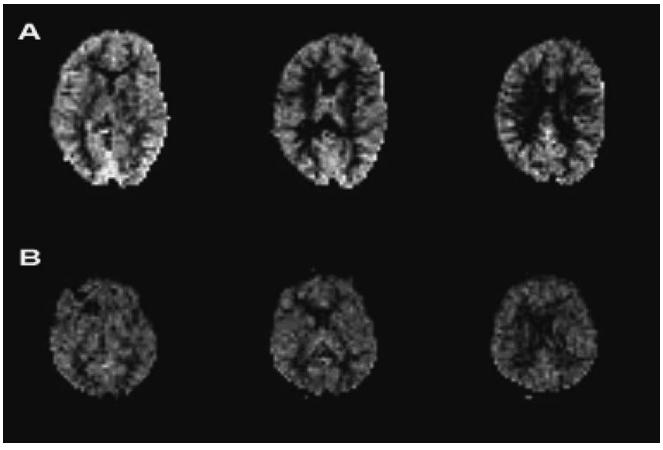


**FIGURE 3.** Comparison of absolute CBF in a normal girl (A) and a female patient with Rett Syndrome (B) of identical ages (10.3 years). Images were acquired at 1.5 T in 8 minutes. The average whole brain CBF is 105 mL/min/100 g for the volunteer and 59 mL/min/100 g for the patient, demonstrating a general reduction in brain metabolism. Notice also the microcephaly of the patient, one of the typical clinical manifestations for this disease.[29]

## Pulsed Arterial Spin Labeling (PASL) Techniques

### Symmetric PASL Techniques

Apart from the continuous ASL techniques, pulsed ASL (or PASL) techniques have met with increasing success, mainly due to the ease of implementation and reduced practical difficulties as compared with those encountered in CASL, such as those related to the long (2–4 seconds) continuous wave-like excitation pulse required. PASL techniques can be separated in two categories, whether the labeling is applied symmetrically or asymmetrically with respect to imaging volume. Generally, the arterial labeling is performed much closer to the acquisition plane in PASL than in CASL, to get an adequate signal-to-noise ratio.

The symmetric PASL sequences are based on a scheme originally proposed by Kwong et al,[10] and independently published by Kim[20] and Schwarzbauer et al,[30] and are referred to as flow-sensitive alternating inversion recovery (FAIR) sequences, according to Kim's acronym.[20] In this particular scheme, an inversion-recovery sequence is performed twice: once with and once without slice-selection gradient to label the arterial spins. The perfusion-weighted signal comes then from the difference in signal intensity due to the absence of inverted arterial spins in the slice-selective experiment with respect to the non-slice-selective inversion recovery sequence.[31,32] Since

both labeled and nonlabeled images are acquired with identical RF pulses, MT effects are counterbalanced over the center slice. However, problems in the control for these effects may arise when using multislice schemes.[33,34] MT-related problems will, however, be less important than in CASL[35] because of the reduced RF power needed in such sequences.

Soon after the publication of the FAIR sequence, several other methods based on similar symmetric labeling were developed:

- In the UNFAIR sequence, meaning "uninverted flow-sensitive alternating inversion recovery," an additional nonselective pulse is applied just after the first inversion pulse to yield noninverted static signal in the volume of interest.[36,37] This sequence, developed independently by Berr et al,[38,39] is also called EST (extra-slice spin tagging).
- The FAIRER acronym refers to two different sequences, aimed at solving different problems: in the first one, FAIRER means "FAIR excluding radiation damping," and consists of a regular FAIR sequence after which a small continuous gradient is turned on to avoid radiation damping effects, affecting mostly animal experiments at high field strength[40,41]; in its second definition, FAIRER means "FAIR with an extra radiofrequency pulse" and consists of a FAIR sequence followed or directly preceded by a 90° RF pulse to null the static signal in the volume of interest. This sequence was designed to be used in pulmonary perfusion imaging, in which cardiac triggering is necessary.[42,43]
- Another version of the FAIR sequence is the FAIREST technique or "FAIR exempting separate $T_1$ measurement," in which a slice-selective saturation recovery acquisition is added to the standard FAIR scheme and used mostly in combined BOLD and CBF fMRI experiments.[44]
- To achieve perfusion quantification with a short repetition time (TR), Pell et al modified the original implementation of the FAIR sequence by performing a global (nonselective) saturation pulse prior to the actual FAIR sequence.[45]
- Finally, in the BASE sequence, meaning "unprepared BAsis and SElective inversion," a selective inversion-recovery sequence and a sequence without any preparation pulse are alternatively acquired, and perfusion is calculated from the expected signals coming from both experiments.[46]

### Asymmetric PASL Techniques

Apart from these symmetrical schemes, another type of PASL techniques has been developed, based on an original sequence called EPISTAR for "echo-planar imaging with signal targeting by alternating radiofrequency pulses."[19] In EPISTAR, the tagging of arterial water magnetization is performed using an inversion pulse in a slab proximal to the volume of interest, after (or before) saturation of the static spins to avoid any contamination of the labeling slab into the measured volume. In the control experiment, the slab is positioned at the same distance distally to the volume of interest, using a simple polarity inversion of the slab-selective gradient. This controls for magnetization transfer effects in a way similar to the original CASL sequence.[11] Based on this original sequence, the following other schemes have been proposed:

- First, the original EPISTAR sequence has been modified by its authors to render it multislice capable.[47] In this second version of EPISTAR, the labeling inversion pulse is replaced by an adiabatic fast passage inversion pulse of twice the length of a conventional 180° pulse, leading to an inversion of the arterial magnetization, while the control scan is composed of two 180° pulses of half the length of the labeling one canceling each other and therefore leaving the spins uninverted in a way similar to the sinusoidal CASL control.
- In the PICORE sequence (proximal inversion with control for off-resonance effects), the labeling experiment is similar to that of EPISTAR while the slab-selective labeling gradient is turned off during the control experiment, therefore controlling for off-resonance MT effects in the central slice of the volume of interest.[35]
- In the TILT sequence (transfer insensitive labeling technique), both labeling and control experiments are performed using two self-refocusing 90° pulses; however, with the phase of the second pulse shifted by 180° in the control experiment, therefore yielding a $90° - 90° = 0°$.[48,49] This scheme allows controlling for MT artifacts over a wide range of frequencies, as both $90° + 90°$ and $90° - 90°$ produce identical MT effects, in a way similar to the sinusoidal modulation in continuous arterial spin labeling[28] or to the modified EPISTAR technique.[47]
- Finally, another scheme has been developed recently, using a "Double Inversion with Proximal Labeling of bOth tagged and control iMAges" (DIPLOMA).[50] In this sequence, the tagging is performed by two consecutive inversion pulses: the first one applied off-resonance, without gradient selection, and therefore inducing only MT effects, and the second one being a slab-selective on-resonance pulse inverting the spins in the region of interest. In the control experiment, two consecutive inversion pulses are played out on-resonance, inducing identical MT effects but no net change in the magnetization, in a way similar to the BASE sequence.[46]

### Technological Improvements: A Clear Definition of the Bolus

In most of the PASL techniques described above, one of the major technical difficulties in getting an absolute quantification of the CBF (see next section) comes from the potentially variable delay or arterial transit time $\delta t$ taken by the blood to travel between the labeling slab and the measurement volume. In an attempt to improve the definition of the bolus and therefore simplifying perfusion quantification, Wong et al[35,51,52] came up with simple modifications of PASL sequences that circumvent the problem of variable $\delta t$ by the introduction of additional saturation pulses. Their methods, dubbed QUIPSS

(I & II) for "QUantitative Imaging of Perfusion using a Single Subtraction" simply add a slab-selective 90° dephasing pulse after a time $TI_1$ in the volume of interest (for the first version) or in the same position as the labeling bolus (in the 2nd version). In the QUIPSS II approach in particular, the bolus width and transit time can be regulated in a way similar to CASL, using the saturation pulse to limit the length of the tag. By carefully timing the signal detection after the saturation pulse, transit-time insensitive perfusion images can be acquired, even for multiple slices. Furthermore, the use of a saturation pulse in both labeled and control acquisitions reduces the artifactually high perfusion-like signal coming from remaining labeled intravascular spins.

A further improvement has recently been introduced by Luh et al,[53,54] in which the saturation pulse is repeatedly applied at the distal end of the labeled volume to improve both the definition of the tagged slab, as well as the cancellation of intravascular signal. The method is called Q2TIPS for "QUIPSS II with Thin-slice $TI_1$ Periodic Saturation."

## Dynamic and Pseudo-Continuous ASL Techniques

One of the drawbacks of ASL, especially when applied to functional MRI (see next Section on Neuroscience Applications) is its relative low inherent temporal resolution, due to the subtraction process involved. Based on this consideration, Wong et al[55] showed that by acquiring the images at an early TI, one gets the perfusion signal from the previous repetition, thereby improving the nominal temporal resolution of PASL[35] by a factor of 2. The conditions to perform such an experiment can be summarized as follows: $TR > \tau$, $TI > \tau + \delta t_{max}$, $TI - TT < \delta t_{min}$, with $\tau$ = temporal width of the bolus, $\delta t_{min}$ (resp $\delta t_{max}$) = minimum (resp. maximum) arterial transit time from the bolus slab to the imaging volume.

Based on a similar observation, Silva and Kim proposed a modified CASL technique, in which short acquisitions are interleaved with an RF labeling pulse in such a way that the labeling duty cycle is still large enough to get a decent labeling efficiency. The control scans are then performed in a separate experiment. In that implementation, they used a TR of 108 milliseconds, with a labeling time of 78 milliseconds for a total readout time (using EPI) of 30 milliseconds.[56]

Using a similar method, Barbier et al[57,58] came up with a dynamic ASL (DASL) technique, in which the response of the tissue magnetization to a periodically varying labeling pulse is measured. This technique alleviates the use of a control experiment to observe the effect of the ASL pulse on the tissue; rather, the tissue response function is directly fitted to a theoretical model, providing a simultaneous estimation of both CBF and arterial transit time in a single measurement.

## Nonsubtraction Methods

Finally, another class of methods has recently been introduced in which perfusion-weighted images can be obtained without the need of a control acquisition. These nonsubtraction methods are based on the concept of background suppression using multiple inversion pulses,[59] first introduced for ASL techniques by Ye et al for multishot three-dimensional perfusion imaging.[60] There are mainly two sequences published for single-shot nonsubtraction spin labeling techniques:

- The first one, dubbed SEEPAGE for "Spin Echo Entrapped Perfusion image," starts with a 90° selective pulse, followed by a train of 180° pulses maintaining the tissue magnetization around zero. The train of pulses is maintained long enough for the non-saturated blood to enter in the slice and provide a perfusion signal.[61]
- In the second one, called SSPL for "Single-Shot Perfusion Labeling," a double-inversion recovery pulse is applied to null both CSF and tissue inside the volume of interest, while keeping the perfusion signal minimally perturbed.[62]

Both methods have however the drawback of being difficult to quantify.

# ABSOLUTE QUANTIFICATION IN ASL

## Equations for CBF Quantification

To get an absolute quantification of CBF from ASL measurements, it is necessary to modify the Bloch equations to include the exchange terms between the static tissue magnetization and the flowing labeled arterial magnetization[13]:

$$\frac{dM_T(t)}{dt} = \frac{M_T^0 - M_T(t)}{T_{1T}} + f\left(M_A(t) - \frac{M_T(t)}{\lambda}\right) \qquad (3)$$

with $M_T$ = tissue magnetization, $M_T^0$ = steady state equilibrium value of $M_T$, $T_{1T}$ = tissue longitudinal relaxation rate, and $M_A$ = arterial magnetization per ml of blood and $f$ = CBF in (mL/g/s). This equation is valid under the following assumptions[63]:

- That perfusion is provided by an uniform plug flow to the tissue.
- That exchange between labeled water and tissue magnetization can be modeled as a single well-mixed compartment, more particularly that the venous concentration of labeled magnetization is equal to the tissue concentration divided by the blood-brain partition coefficient $\lambda$, ie, $M_v(t) = M_T(t)/\lambda$.

Originally, the first models used for absolute quantification of ASL did not take into account the effect of arterial transit time $\delta t$ in the measured signal.[10,11,13,24,31] Buxton et al[63] demonstrated theoretically that it is one of the most important parameters needed for the quantification of both PASL and CASL techniques.

Generally, a supplementary condition is also implied to get an analytical solution to Eq. 3: that labeled water is completely and spontaneously extracted from the intravascular space as it enters the tissue, ie, that labeled blood magnetiza-

tion relaxes with the longitudinal relaxation time of arterial blood $T_{1B}$ until it reaches the tissue, and with $T_{1T}$ thereafter. With these assumptions, the general solution for PASL[63] and CASL[64] techniques can written as:

**For PASL**

$$\Delta M_T(t) = \begin{cases} 0 & 0 < t < \delta t \\ 2\alpha \dfrac{M_T^0}{\lambda} f(t-\delta t) e^{-R_{1B}t} q_{PASL}(t) & \delta t < t < \tau + \delta t \\ 2\alpha \dfrac{M_T^0}{\lambda} f\tau\, e^{-R_{1B}t} q_{PASL}(t) & \tau + \delta t < t \end{cases} \quad (4)$$

with

$$q_{PASL}(t) = \begin{cases} \dfrac{e^{\Delta R_1 t}(e^{-\Delta R_1 \delta t} - e^{-\Delta R_1 t})}{\Delta R_1 (t-\delta t)} & \delta t < t < \tau + \delta t \\ \dfrac{e^{\Delta R_1 t}(e^{-\Delta R_1 \delta t} - e^{-\Delta R_1 (\tau+\delta t)})}{\Delta R_1 \tau} & \tau + \delta t < t \end{cases} \quad (5)$$

and $R_{1B} = (T_{1B})^{-1}$ is the longitudinal relaxation rate of arterial blood, $\Delta R_1 = R_{1B} - R_{1app}$ is the difference between the relaxation rate of arterial blood and apparent relaxation rate of the tissue, and $R_{1app} = R_{1T} + f/\lambda$ is the apparent relaxation rate of the tissue, which depends on CBF.

**For CASL**

$$\Delta M_T(t) = \begin{cases} 0 & 0 < t < \delta t \\ 2\alpha \dfrac{M_T^0}{\lambda} f T_{1app} e^{-R_{1B}\delta t} q_{CASL}(t) & \delta t < t < \tau + \delta t \\ 2\alpha \dfrac{M_T^0}{\lambda} f T_{1app} e^{-R_{1B}\delta t}\, e^{-R_{1app}(t-\tau-\delta t)} q_{CASL}(t) & \tau + \delta t < t \end{cases} \quad (6)$$

with

$$q_{CASL}(t) = \begin{cases} 1 - e^{-R_{1app}(t-\delta t)} & \delta t < t < \tau + \delta t \\ 1 - e^{-R_{1app}\tau} & \tau + \delta t < t \end{cases} \quad (7)$$

The main reason to express these two results (Eqs. 4 and 6) using a dimensionless $q$ function is to show the similarity between the equations governing both CASL and PASL methods. It can be demonstrated that CASL measured in peak steady state conditions provides a perfusion signal $\Delta M_T$ at most $e$ times larger than PASL, if $T_{1app} = T_{1B}$.[63,65] These $q$ functions describe also the effects of the different relaxation times as well as the venous clearance of the labeled magnetization in PASL, and the approach to steady state in CASL. In both cases, and after a sufficiently long time in CASL, both expressions are close to 1 and can therefore be neglected in a first approximation.

## The Effect of Magnetization Transfer

Several papers have dealt with the effects of magnetization transfer on the absolute quantification.[64,66–68] But the most complete theoretical description is depicted in a paper by McLaughlin et al.[67] In this paper, the authors investigated in particular the questions about both terms in the ratio $\Delta M(t)/T_{1app}$ that appears in the equations providing $f$ in CASL techniques. They based their observation on the following equations describing a four-pool model:

$$\begin{cases} \dfrac{dM_T(t)}{dt} = \dfrac{M_T^0 - M_T(t)}{T_{1T}} - k_f M_T(t) + k_b M_M(t) \\ + f E(f) \left( M_A(t) - \dfrac{M_T(t)}{\lambda} \right) \\ \dfrac{dM_M(t)}{dt} = \dfrac{M_M^0 - M_M(t)}{T_{1M}} + k_f M_T(t) - k_b M_M(t) \end{cases} \quad (8)$$

In which $E(f)$ is the water extraction fraction, depending on the CBF, the index $M$ refers to the magnetization of the bound macromolecular pool,[22] and $k_f$ and $k_b$ are the forward and backward magnetization transfer rate constants between the free and bound water pool, respectively, obeying the following relation at equilibrium: $k_f M_T^0 = k_b M_M^0$. Without entering too much into the details of this model, the general flavor of its results is that under a wide range of conditions, reasonable and consistent choices for $\Delta M(t)$ and $T_{1app}$ should facilitate calculation of correct values for CBF in CASL experiments.

## Restricted Exchange and Multiple Compartment Modeling

Another possible improvement of the original model based on the Kety-Schmidt equations for ASL is to include the effects of restricted water exchange between intravascular and extravascular compartments (ie, finite capillary water permeability) as well as capillary contributions to the ASL signal.[69–72] In these four papers, different additional terms have been added to the original equations, and different values of underestimation or overestimation of CBF have been found, depending on the assumptions made. Zhou et al[70] used a 2-compartment model in its expression similar to Eq. 8, with the exchange terms expressed between intravascular and extravascular compartments, and applied their results to measure CBF from a FAIR sequence at 4.7 T. They obtained a good correlation between their FAIR measurements and microsphere measurements of perfusion. St. Laurence et al[71] worked out similar equations and obtained similar results for CASL, showing that generally, the single-compartment model provides relatively accurate CBF values at 1.5 T (within 5%) for gray matter. Parkes and Tofts[69] found an overestimation of CBF in gray matter at 1.5 T of more than 60% (and 17% in white matter) in FAIR-like sequences. They attributed the differences of their model with the previous ones to differences in

the choice of $T_{1B}$ and some differences in the modeling of the venous outflow.

## ARTIFACTS AND PROBLEMS

### SNR and Imaging Problems

One of the major problems of ASL techniques is their intrinsic low signal-to-noise ratio (SNR). Indeed, the measured $\Delta M/M_0$ is often on the order of 1% or less, and subtraction errors are frequent, often caused by improper selection of the inversion width[73] or motion artifacts in clinical studies of difficult patient populations.[74] For this reason, several background-suppression schemes have been developed based on the possibility to cancel the signal of more than one tissue using multiple inversion pulses.[59] This background-suppression method has been used for nonsubtraction ASL,[61,62] as well as for multishot three-dimensional PASL[60] and CASL.[9] Other ways to increase the SNR in perfusion-weighted images have been proposed, such as maximizing the SNR in both control and labeling acquisitions, for example, by carefully choosing the minimal usable $B_1$ field in CASL to minimize MT effects as much as possible.[75] But the best way to ensure a proper subtraction of labeled from control scans is to use fast (single-shot) imaging techniques. In most applications of ASL in the brain, single-shot EPI[10,19,20] or spiral imaging[34,60,76,77] has been used. However, strong susceptibility artifacts, especially at the basis of the brain, render such readouts less than perfect. Therefore, other readout techniques have been proposed to alleviate this problem, based on line-scan,[78,79] or fast-spin echo[80–82] imaging. In applications of ASL outside the brain, very few studies have used single-shot EPI methods, mainly in kidney perfusion imaging[83] or musculoskeletal perfusion imaging.[84–86] Instead, simple gradient-echo or fast spin-echo-based sequences, both of which are susceptibility insensitive techniques, have been used for measuring cardiac perfusion,[87–91] skeletal muscle perfusion,[92–94] pulmonary perfusion,[42,43,95–98] or perfusion in the urogenital system.[39,80,99–102]

### Transit Time and Vascular Artifacts

Another main problem of ASL techniques comes from the remaining labeled signal in the vasculature. Upon subtraction of labeled from control experiments, remaining inverted blood will result in spuriously high perfusion values, especially in presence of a low resolution imaging technique. For this reason, the first CASL sequences had already implemented small diffusion gradients (diffusion $b$-value = 1–10 seconds/mm$^2$) to eliminate any remaining arterial signal.[13,103] Based on a similar idea, Pell et al[104] implemented a scheme in which a DEFT diffusion preparation sequence is performed prior to a Turbo-FLASH readout. Recently, by comparing the signal obtained with and without crusher gradients, Wang et al could obtain an estimate of the arterial transit time.[105]

Another solution to strongly reduce the effects of intravascular contamination is to adjust the predelay between continuous labeling and readout.[28,64] This latter method has the advantage of not reducing the already small SNR available and is easier to implement. Furthermore, it renders the method insensitive to variable transit times. In PASL, the QUIPSS-based techniques are effective in a similar way.[51–53]

### RF Pulse Shapes

Finally, one of the major implementation problems encountered, especially in PASL techniques, is related to the use of very well-defined inversion pulses, as profiles not sharp enough will result in a reduced labeling efficiency as well as possible contamination by the labeling pulse of the volume of interest.[49,106–109] For this reason, very sharp labeling pulses are needed, mainly adiabatic fast passage[47,106] or frequency offset-corrected inversion pulses.[36,108,110] Finally, the TILT sequence uses self-refocusing concatenated 90° Shinar-Leroux optimized RF pulses[111] to maintain the profile efficiency of the 90° pulses.[49] One drawback of this technique is that it can only be used under very good shimming conditions.[50]

## APPLICATIONS IN NEUROSCIENCE

### Functional ASL Versus fMRI

One of the original reasons for the development of ASL was the drive to develop a fully noninvasive technique allowing measuring the local changes in CBF related to a functional task.[19,20,112] Indeed, ASL techniques developed in parallel with functional MRI (fMRI) techniques based on the blood oxygen level-dependent (BOLD) contrast.[112–114] Similarly to fMRI, early functional ASL studies measured perfusion changes in primary motor[20,32,35,115–118] or visual[46,119–122] activation tasks. Only few studies have been used in cognitive tasks.[123] However, fundamental differences exist between both techniques: while $T_2$*-weighted BOLD fMRI measures an epiphenomenon secondary to local increases in oxygenation, ASL provides a direct absolute measurement of CBF changes. ASL should be therefore more reproducible among subjects and generally over longer periods of time,[124–126] despite its intrinsic lower SNR.[34,127,128] Furthermore, it is less prone to artifacts coming from large draining veins, as its signal is mainly of arteriolar and microvascular origin[129,130] and is therefore usable for very high-resolution functional mapping, such as columnar resolution functional ASL.[131] Then it has to be noted that at very high field (9.4 T), functional areas depicted by both spin-echo BOLD and CBF were found to be pretty well co-localized, which can be attributed to the complete loss of coherence of blood signal for long echo times at such high field strength.[132] However, the necessity of the subtraction procedure makes ASL less favorable for event-related fMRI than BOLD, necessitating the use of complex reordering procedures[133,134] or of no-subtraction ASL techniques.[62] A possible way to increase the temporal resolution in ASL can be

 

achieved using a so-called stroboscopic acquisition, in which the frequency of the activation paradigm is shifted with respect to the frequency at which the data are acquired.[135]

On the other hand, CASL is not as easy to interpret as BOLD. In particular, changes in arterial transit time have been measured using ASL and can be misinterpreted as elevated perfusion upon activation.[136–140] In particular, Gonzales-At et al showed that depending whether the model used a single transit time or a transit time distribution, the transit times varied from 10% to 25% during motor or visual activation in functional CASL experiments.[137]

Furthermore, these changes in transit time are different in each voxel and are dependent on the arterial content of the voxel.[139,140] As a demonstration of this effect, Figure 4 depicts the arterial transit time at which voxels in the visual cortex show maximum cross-correlation with a simple visual stimulus paradigm using the Turbo-TILT sequence (see Emerging Techniques).[140] At short delay times, the maximum cross-correlation is located near the areas surrounding the central sulcus, where large arteries are present. For longer delay times, this area is shifted to the posterior and lateral part of the visual cortex.

Generally, detection of functional ASL changes cannot be compared directly to BOLD fMRI, as the noise characteristics of ASL are very different from those of BOLD as shown by Wang et al[141]; they found that fMRI time series are more or less independent in time and did not show spatial coherence varying across temporal frequencies. This finding has implications for the spatial smoothing of functional perfusion data.

## Metabolic and Oxygen Consumption Studies

One of the first demonstrations of a correlation between oxygen metabolism and blood flow was demonstrated in the skeletal muscle by Toussaint et al.[94] using $^{31}P$ spectroscopy as a direct measure of muscle metabolism.

In the brain, Kim and Ugurbil demonstrated using combined FAIR and BOLD experiments that changes in oxygen consumption during activation are very low.[127] Later, the same group demonstrated a linear relationship between CBF and BOLD changes in a graded visual stimulation paradigm.[120] These experiments were repeated and reinterpreted using a $CO_2$-based titration procedure[142] to obtain independently absolute metabolic rates of oxygen by the same group[143] and by Hoge et al.[144,145] A more detailed study of the effects of hyperoxia, hypercapnia, and hypoxia on both CBF and interstitial oxygen tension was also published by Duong et al.[146] Similar validation experiments were performed using CASL on a rat model by Silva et al.[147]

ASL has been also used to further study the temporal characteristics of activation-related CBF changes. In particu-

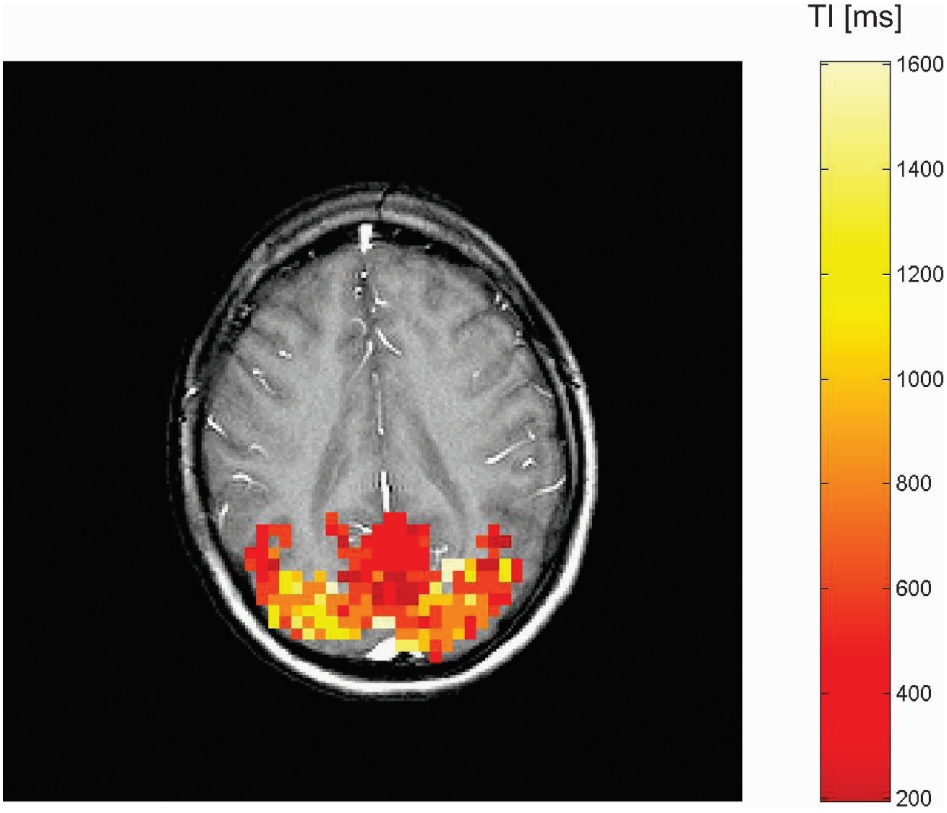


**FIGURE 4.** Application of Turbo-TILT to functional imaging.[140] The color map highlights the postlabeling delay at which the voxels in the visual cortex show maximum cross-correlation with a simple visual stimulus paradigm. At short postlabeling delay times, the maximum cross-correlation is located near the areas surrounding the central sulcus. For longer delay times, this area is shifted to the posterior and lateral part of the visual cortex.

lar, based on the mismatch between the temporal characteristics of the BOLD and ASL signals following brain activation, Buxton et al[116] developed a simple biomechanical model explaining these changes, the so-called "balloon model." Concurrently, ASL was used by Silva et al[148] to understand the early negative changes in the BOLD signal (called the "early-dip"),[149] which is thought to be closer to the site of activation.[150] However, the authors of this study could not demonstrate any evidence of such early loss in hemoglobin oxygenation preceding the rise in CBF and concluded that increases in CBF and oxygen consumption were likely to be dynamically coupled in their animal model. Other applications of ASL in the determination of the functional characteristics of the BOLD signal included, among others, a study on the linearity of the temporal dynamics of ASL.[151]

### Pharmacological Applications

ASL is also of great interest in the study of various drugs, in both humans and animals, as it does not require the injection of another compound that might interfere with the tested pharmacological agent.[152] Furthermore, ASL provides absolute quantification of a physiological parameter (CBF), unlike T2*-weighted BOLD, in which changes in signal can be interpreted as coming either from changes in oxygen extraction, blood flow, or metabolism. In particular, a twofold to fourfold increase in CBF has been demonstrated after administration of 2-chloroadenosine, a potent cerebrovasodilator, to rats.[153,154] Similarly, elevated CBF was measured in volunteers following injection of acetazolamide.[155] The same drug was also used in measuring the cerebrovascular reserve in patients with ischemic symptoms referable to large artery cerebrovascular stenosis of the anterior circulation.[156] Drugs with opposite effects, such as indomethacin[157,158] or the anesthetic gas isoflurane,[159] have also been tested using CBF in both humans and animals, respectively. Finally, Born et al measured the changes in CBF in the visual cortex in children under sedation,[160] trying to investigate the origin of the negative BOLD signal observed often in such case and found a slight decrease in CBF upon visual activation.

## CLINICAL APPLICATIONS

### Validation of ASL Prior to Clinical Studies

Prior to any clinical application of ASL, several animal studies reported general behavior of these sequences in terms of reproducibility and comparison with "gold-standard" invasive methods. In a study on rats, Zhou et al showed a good correlation between values measured with FAIR and radioactive microsphere CBF measurement methods.[70] Ewing et al also demonstrated a good correlation of local CBF measured by ASL on direct comparison with quantitative autoradiography.[161] Finally, Pell et al recently used the oxygen clearance method and compared it with a PASL technique (FAIR).[162] They also found a very good correlation between CBF values measured by both techniques, although impaired slightly by the large scattering in their FAIR measurements. Furthermore, human studies of cerebral perfusion using ASL have shown good within-subject variation in normal adults,[163] as well as in children.[164] Lia et al[165,166] have compared the results of CBF measured independently in health volunteers by contrast reagent-based techniques to ASL measurements and found good correlation between both techniques ($r = 0.86$ over 8 subjects). Finally, Ye et al have published a study comparing the results of ASL to $^{15}$O-labeled PET and found an extremely good concordance between both methods in the cortical gray matter (ASL: 64 ± 12 mL/100 g/min and PET: 67 ± 13 mL/100 g/min).[167] However, perfusion in the white matter was underestimated, in agreement with what could be expected from theoretical studies using extended models.[71]

As a fully noninvasive method, ASL might be particularly advantageous where a technique not necessitating intravenous injection is required, especially when repeated scans are foreseen. In animal models of transient cardiac arrest, ASL has been successfully used to assess postresuscitation cerebral reperfusion.[168–171] By making repeated ASL measurements, some authors have demonstrated that early resuscitation increased reperfusion after cardiac arrest and improved survival.[168] This technique has now been used to study the effects of different treatment strategies to improve cerebral recovery.[169,171]

### Pediatric Studies

ASL techniques, with better safety and image quality, are attractive for studying cerebral perfusion in the pediatric population and pose less of an ethical problem than nuclear medicine studies.[74,164] Children have generally a higher blood flow than adults with a peak at around 10 years of age.[164,172,173] This higher physiological CBF will lead to increased SNR in ASL and reduce the artifacts caused by slow arterial transit time. Conversely, in dynamic contrast reagent studies in children, the increased CBF, coupled with the reduced total dose of contrast media, would lead to technical difficulties in sampling the first pass bolus.

Recent studies from Wang et al[164] and Oguz et al[74] also found an increase in the cerebral blood flow in normal children compared with adult controls. Furthermore, in the latter report, children with sickle cell disease were identified with reduction in CBF without large arterial disease on MR angiogram, demonstrating the potential for noninvasive prospective identification of children at risk for stroke and other complications.

### Cerebral Ischemia

In animal studies, ASL has been successfully applied to study the effects of complete[174,175] or partial[176] occlusion of

the middle cerebral artery. Early human studies have shown that ASL methods could be successfully applied in acute stroke[177–180] and could be used in acetazolamide challenge test in patients with vascular stenosis.[156,181]

The main problem in cerebral ischemia, as well as in partial or complete arterial occlusion, is the lengthening in transit time due to collateral flow or reduced arterial velocity,[177] sometimes producing artificially elevated signal changes due to remaining labeled magnetization in the large arteries on the affected site. Such effects need to be clearly distinguished from luxury perfusion occurring in chronic stroke patients, such as depicted in Figure 5, in which a 50-year-old man presenting with right hemiplegia and aphasia was scanned more than 1 day after symptom onset. In this case diffusion-weighted and $T_2$-weighted MR images show a hyperintensity in the infracted area, and the CASL images show increased cerebral blood flow from luxury perfusion.

## Tumors

Measurement of tumor blood flow is important for tumor grading and evaluating anticancer treatment effect.[182–184] As example of the use of ASL in tumors, Figure 6 shows clearly increased tumor blood flow in a patient with glioma despite the lack of contrast enhancement on conventional MR imaging. Because of the use of a purely diffusible tracer, ASL techniques may allow absolute quantification unaffected by disrupted blood–brain barrier, a common problem using contrast reagent-based techniques for assessing tumor perfusion, and allows distinction between high- and low-grade gliomas.[184] However, dynamic contrast medium-based techniques are still the preferred technique today because of superior SNR and increased anatomic coverage. Furthermore, patients with brain tumors usually undergo contrast-enhanced scans as part of conventional imaging protocols, and the advent of high field imaging will soon allow measurement of perfusion without the need for an increase in contrast reagent dose.[185,186] ASL may also be useful for repeated studies on the effects of radiation therapy or pharmacological agents (such as nicotinamide) to increase tumor blood flow and also to assess different therapies treatment regimens in both intracranial and head and neck malignancies.[183,187,188]

## Other Cerebral Diseases

ASL has been used in many other diseases affecting the central nervous system, including Alzheimer disease,[189,190] epilepsy,[82,191] clinical depression,[192] rare diseases, such as postpartum vasculopathy,[193] Rett syndrome,[29,194] or Fabri disease,[195] as well as traumatic injury in rodent models.[153,196] A summary of the clinical findings in patients is presented below.

In both studies on Alzheimer's disease, either using PASL[190] or using CASL,[189] focal areas of hypoperfusion were consistently found in patients as compared with the normal controls, mainly in the posterior temporoparietal and occipital areas[190] as well as in frontal and posterior cingulate cortices.[189] These deficits correlated with the severity of dementia.

Two studies have also been reported on changes in the CBF of patients with temporal lobe epilepsy (TLE), using either CASL (191) or PASL (82). Both studies could find local or lateralized areas of reduced CBF in the mesial temporal lobe related to TLE. Interestingly, both studies found significant correlation between ASL results and PET measurements of CBF[82] or glucose metabolic rate.[191]

A recent PASL study investigated the links between depression, cardiac disease, and CBF.[192] For this study, the authors acquired two axial slices through the upper and lower halves of the lateral ventricles. On the upper slice, CBF was significantly lower on the left side in the depressed subjects than in the control group, suggesting that relative cerebral hypoperfusion may underlie depression in elderly cardiac patients.

Rett Syndrome is a rare X-linked genetic disease, leading to developmental regression and deceleration of head growth accompanied by loss of communication skills, seizures, respiratory abnormalities, and peculiar stereotyped hand-wringing behavior.[29] In both studies of this disease, ei-

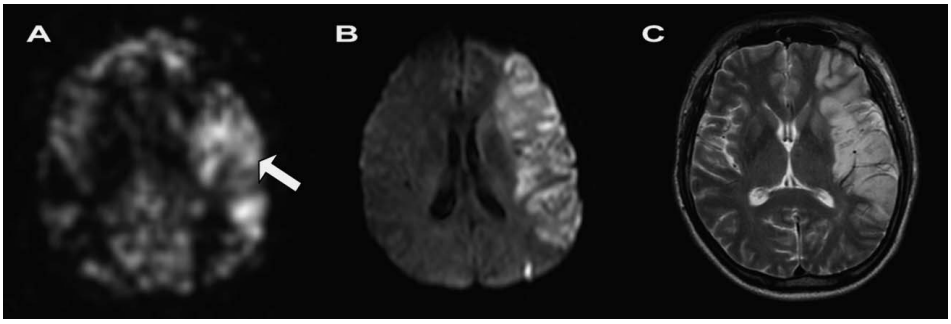


**FIGURE 5.** CASL (A), isotropically diffusion-weighted (DW) (B), and $T_2$-weighted (C) images of a 50-year-old man with recent onset of right hemiplegia and aphasia. All images were acquired at 3.0 T. The CASL images were acquired in 6 minutes 40 seconds. The DW and $T_2$-weighted MR images show hyperintensity in the infarcted area, while the perfusion-weighted CASL image shows increased cerebral blood flow from luxury perfusion (arrow). Note that the DW image is not acquired at the same angle as the two other images.

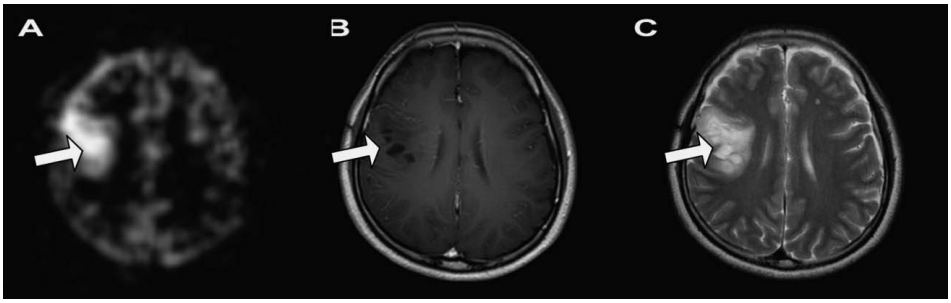


**FIGURE 6.** CASL (A), postcontrast $T_1$-weighted (B), and $T_2$-weighted (C) images of a 32-year-old woman with seizures on follow-up for right frontal glioma. All images were acquired at 3.0 T. The CBF-weighted CASL image was acquired in 3 minutes, and only 19 averages were included to form this image.[74] Although the tumor does not enhance after intravenous contrast injection (Gd-DTPA), the CASL perfusion-weighted image demonstrates a clear increase in cerebral perfusion.

ther with PASL[29] or with CASL,[194] reduced general perfusion was observed, with a marked reduction (30%) in the frontal lobe, probably related to their delayed developmental state. In Fabry disease, Moore et al found that CBF was elevated in the posterior circulation, especially in the thalamus.[195]

### Other Clinical Non-Brain Indications

Although the majority of applications have been focused on cerebral perfusion, ASL methods have been successfully applied to other organs, with interest in pulmonary,[42,43,95–98,197–206] cardiac,[11,87–91,207] renal,[39,83,99,102,208] breast,[209] uterine,[210] or ovarian[100,101] perfusion studies.

Pulmonary ventilation or perfusion MR studies, particularly quantitative methods, would be desirable to improve spatial resolution and avoid the radiation dose associated with classic radionuclide studies used to assess pulmonary embolism. ASL techniques were successfully applied in studies of normal volunteers[95,96,98,203] as well as in animals[197,201] and humans with perfusion deficits,[97] lung transplantation,[202] and cystic fibrosis.[206]

Myocardial perfusion was studied in isolated[207] and intact animal hearts[90,91] to assess vasodilation induced by pharmacological agents. Human investigations show promising potential of ASL to become an important noninvasive and easily repeatable method to study changes in cardiac blood flow in patients with coronary disease.[211]

Several studies of ASL in renal diseases have been performed. In a study of kidney transplant rejection, Wang et al[99] found that reduction in renal cortical perfusion rate determined by MRI was significantly correlated with histologic rejection. Other reduced renal perfusion due to renal vascular disease[39,83] have also been described.

## EMERGING TECHNIQUES

### High-Field Clinical ASL

In the past few years, moderate and high field MR systems ($\geq$ 3.0T) have been introduced in the clinical settings. Advantages of higher field strength have been demonstrated for magnetic resonance angiography,[212] fMRI,[213] and magnetic resonance spectroscopy.[214] An expected twofold SNR increase proportional to the magnetic field strength is the most appealing feature of 3T MR imaging, but other properties such as increased $T_1$ relaxation times may also provide great advantages for ASL. Indeed, most CASL sequences use a TR in the order of 5 seconds, with the shortest possible echo times, resulting in proton density weighted images. Therefore, both the increase in $T_1$ and decrease in $T_2$ expected at 3T[215] will not affect the image contrast, and the native perfusion-weighted images will plainly profit from a twofold increase in SNR.[216,217] Furthermore, the increase in arterial blood $T_{1b}$ from 1400 ms[218] at 1.5 T to 1680 ms[219] at 3.0 T shall increase the contrast-to-noise ratio of the images by approximately 20% to 30%, depending on the imaging parameters. In a study by Franke et al,[220] both increase in signal as well as in $T_{1b}$ were found to be the main contributors for the increase in CNR in ASL when going to higher field strength. Therefore, a reduction of the scan time by a factor of up to four for identical imaging parameters is expected when going from 1.5 T to 3.0 T; alternatively, this increase in SNR may be traded for increased image resolution.

In PASL sequences, usually an inversion (eg, FAIR) or presaturation (EPISTAR, TILT, QUIPSS) pulse is followed 1 to 2 seconds later by the acquisition sequence. These pulses will therefore be the main determinant of the contrast in the native (nonsubtracted) image, which will show in most cases a $T_1$ weighting. For this reason, the expected SNR gain is less than that of CASL sequences[217] at high field strengths. However, the increased $T_{1b}$ will still contribute to an increase in SNR.

### ASL at Multiple Inversion Times

In the majority of PASL or CASL studies, a single delay time TI between labeling and image acquisition is used to estimate CBF. In such cases, the effects of arterial transit time on the CBF estimation are difficult to evaluate and can potentially cause errors in calculated perfusion values.[31,52,64] This is especially true for patients with stroke and steno-occlusive disease of the carotid arteries for whom the labeled blood flowing

 

via collateral vessels will cause an increased transit time in the affected area.

A possible approach to solve the transit time problem is based on the observation that, instead of minimizing the effect of transit time, this physiologically important hemodynamic parameter can also be measured in addition to CBF measurements by performing multiple ASL experiments at various TIs between ASL labeling and MR acquisition. Buxton et al. introduced the theoretical basis of this multiple TI method and proved the principles with an EPISTAR-like technique.[63] Gonzalez-At et al proposed a similar method based on a CASL sequence and applied it to fMRI studies.[137] Several studies have investigated the shape of ASL hemodynamic response curves, with the amount of ASL signal plotted against TI.[34,103,138] Generally, an increase of the perfusion-weighted signal is found at short TI for PASL sequences caused by the arrival of the labeled blood through the arterial system (Fig. 1), followed by a decrease at longer TI, caused by a combination of washout of the tracer and $T_1$ relaxation, seen in both PASL and CASL[137] (see Absolute Quantification). The main drawback of ASL at multiple inversion times is the considerably longer scan time than for single delay experiments, often rendering this technique impractical, especially in difficult patient populations. Recently, Inflow Turbo Sampling FAIR (ITS-FAIR) and Turbo TILT were introduced, both of which allow absolute quantification of CBF and arterial transit time in a single scan.[139,140,221] Both techniques acquire a series of images at increasing delay times after one single inversion pulse by combining a pulsed ASL with a repeated small flip angle gradient echo sampling strategy, in a way similar to the Look-Locker technique used for fast $T_1$ mapping.[222] When applied to PASL sequences, the Look-Locker acquisition train allows monitoring the dynamics of blood inflow and tissue perfusion at high temporal resolution (50–200 milliseconds). A clinical example of transit time and CBF maps obtained with the turbo tilt method is demonstrated in Figure 7.

## Selective ASL Methods

Thus far, most ASL techniques have been used to measure tissue perfusion of the brain by nonselectively labeling of all of the brain feeding arteries. Edelman et al. introduced selective labeling with a sagittal inversion slab for angiography; however, no flow territory mapping or CBF quantification was performed in these studies.[223] As mentioned earlier, local surface coils in CASL experiments can also be used for selective labeling of the right and left common carotid artery separately.[24–27] Because the surface coils only allow for labeling of superficial arteries, this method is restricted to selective labeling of either internal carotid arteries (ICA), and no separate labeling of the posterior circulation can be achieved.

Using a PASL technique similar to that of Edelman et al,[223] Eastwood et al selectively labeled either the right or left carotid artery systems by alternating the application of spatially selective inversion pulses in sagittal orientation.[224] However, they were not able to get an absolute quantification using this technique. Recently, another PASL method for selective labeling of ICAs and basilar artery was implemented using two-dimensional labeling pulses forming a pencil beam profile.[225] By planning this pencil beam with a gaussian profile parallel to the slices of interest and below the circle of Willis, 2 to 4 cm of the left or right ICA or basilar artery could be labeled. However, a significant contamination of the perfusion territories of the nonlabeled arteries was still present and no CBF values were obtained, due to the complex labeling scheme used and the absence of global control for magnetization transfer effects.

Hendrikse et al[226] recently developed another technique based on TILT,[48] called regional perfusion imaging (RPI). With RPI, selective labeling is achieved by using the sharp labeling profiles of the concatenated TILT labeling pulses[49] and by interactively planning the spatially selective inversion slabs.[226] RPI allows CBF quantification because of its inherent global control for MT effects independent of the angulation of the labeling slab.[48,49] As a potential clinical use of this tech-

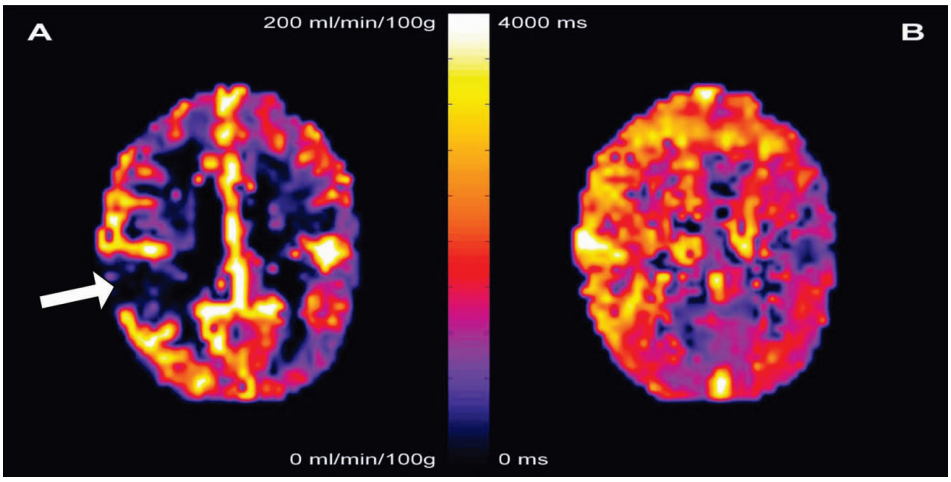


**FIGURE 7.** Absolute CBF (A) and $\tau_D$ = time for the lower edge of the bolus to reach the tissue (B) of a patient with right carotid occlusion and small right side infarction (arrow). It can be seen that the whole right hemisphere, although not suffering from a reduced blood flow, presents with a significant increase in $\tau_D$, indicating delayed cerebral perfusion through co-lateral circulation.

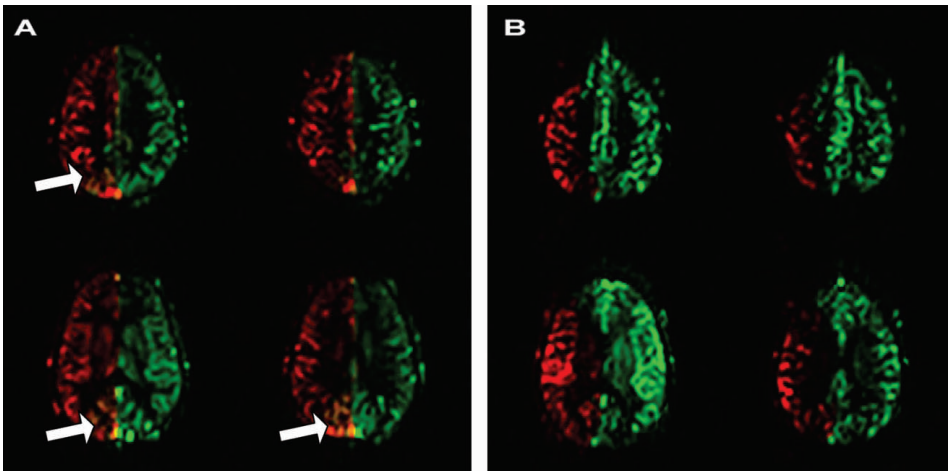


**FIGURE 8.** Regional perfusion imaging (RPI) of a normal volunteer (A) and of a patient after EC-IC bypass surgery (B). In this picture, CBF coming from the right ICA (for the volunteer) and from the bypass (for the patient) are color-coded in red, and CBF coming from the left ICA is color-coded in green. Notice that the posterior circulation is coming from both sides in the volunteer, while both territories are perfectly distinct in the patient. This probably reflects a mixing of flow from both ICAs through the circle of Willis (CoW) in the volunteer, while the patient's bypass graft is attached at a location distal to the CoW.

nique, RPI images in a control subject and a patient after high flow extracranial to intracranial bypass surgery are demonstrated in Figure 8.

## Velocity-Encoded ASL

In general, most ASL techniques described so far are based on the proximal labeling of arterial magnetization followed by its measurement in the tissue of interest after a certain delay time. As expressed earlier, the main problem of such techniques is the finite arterial transit time between the labeling slab and the volume of interest. This transit time can be considerably longer in patients suffering from arterial occlusion, stroke, or arteriovenous malformations, for example. Furthermore, the transit time also depends on the actual relative position of the tissue to the labeling plane or slab. That is, the delay will generally be longer for more distal slices.

In an attempt to render ASL techniques independent from these arterial transit delays, another class of arterial spin labeling techniques has recently been introduced, in which arterial spins are labeled everywhere according to their velocity[227,228] and termed later velocity-selective ASL by Wong et al.[229] In this method, a series of nonselective 90°-180°-90° pulse sequence is used (DEFT sequence), with interleaved gradients to select spins of a particular velocity, in a way similar to MRI sequences used to obtain quantitative flow measurements in large vessels.[230] For the control experiment, the same sequence is repeated with very low gradients. The main difference between this method and other ASL techniques is that flowing spins are labeled everywhere, including in the volume of interest, therefore minimizing the transit delay time necessary for the blood to reach any region of interest in the organ.

## CONCLUSION

Tremendous improvements have appeared in the field of ASL over the last 12 years. Interestingly, however, most up-to-date methods are still based on the original scheme proposed by Williams et al,[13] except maybe some techniques based on velocity-selective ASL.[227,229] This new way of measuring blood flow has been used widely in animal imaging, small clinical studies, as well as a potential surrogate to BOLD fMRI in neuroscience. From the original brain technique have emerged various methods specifically designed to measure blood flow in a large number of organs.

On the technical side, improvements in the techniques and control for the numerous potential artifacts have permitted the development of reliable multislice perfusion imaging, with a resolution often as good as, or even better than, most nuclear medicine approaches. Despite all these improvements and the continuous research done in this domain, ASL is still an emerging technique per se and has not replaced more invasive procedures for the assessment of blood flow in patients. Among the possible explanations for this are probably the relative complexity of the method and its intrinsic low SNR and relative high sensitivity to motion artifacts. As summarized in this review, some of the latest developments and the advent of high field clinical imagers might change this perception, however, and future advances ahead will definitely bring the robustness needed by this technique to be widely used in the clinics.

## REFERENCES

1. Kety SS, Schmidt CF. The determination of cerebral blood flow in man by use of nitrous oxide in low concentrations. *Am J Physiol*. 1945;143:53–66.
2. Kety SS, Schmidt CF. The nitrous oxide method for the determination of cerebral blood flow in man: theory, procedure and normal values. *J Clin Invest*. 1948;27:467–483.
3. Roberts DA, Rizi R, Lenkinski RE, et al. Magnetic resonance imaging of the brain: blood partition coefficient for water: application to spin-tagging measurement of perfusion. *J Magn Reson Imaging*. 1996;6:363–366.
4. Powers WJ, Grubb RL Jr, Darriet D, et al. Cerebral blood flow and cerebral metabolic rate of oxygen requirements for cerebral function and viability in humans. *J Cereb Blood Flow Metab*. 1985;5:600–608.

5. Raichle ME. Measurement of local cerebral blood flow and metabolism in man with positron emission tomography. *Fed Proc*. 1981;40:2331–2334.
6. Maeda T, Matsuda H, Hisada K, et al. Three-dimensional regional cerebral blood perfusion images with single-photon emission computed tomography. *Radiology*. 1981;140:817–822.
7. Barbier EL, Lamalle L, Decorps M. Methodology of brain perfusion imaging. *J Magn Reson Imaging*. 2001;13:496–520.
8. Calamante F, Thomas DL, Pell GS, et al. Measuring cerebral blood flow using magnetic resonance imaging techniques. *J Cereb Blood Flow Metab*. 1999;19:701–735.
9. Alsop DC. Perfusion magnetic resonance imaging. In: Atlas SW, ed. *Magnetic Resonance Imaging of the Brain and Spine*, 3rd ed, vol. 1. Philadelphia: Lippincott Williams & Wilkins, 2002:215–238.
10. Kwong KK, Chesler DA, Weisskoff RM, et al. MR perfusion studies with T1-weighted echo planar imaging. *Magn Reson Med*. 1995;34:878–887.
11. Detre JA, Zhang W, Roberts DA, et al. Tissue specific perfusion imaging using arterial spin labeling. *NMR Biomed*. 1994;7:75–82.
12. Silva AC, Williams DS, Koretsky AP. Evidence for the exchange of arterial spin-labeled water with tissue water in rat brain from diffusion-sensitized measurements of perfusion. *Magn Reson Med*. 1997;38:232–237.
13. Williams DS, Detre JA, Leigh JS, et al. Magnetic resonance imaging of perfusion using spin inversion of arterial water. *Proc Natl Acad Sci USA*. 1992;89:212–216.
14. Dixon WT, Du LN, Faul DD, et al. Projection angiograms of blood labeled by adiabatic fast passage. *Magn Reson Med*. 1986;3:454–462.
15. Zhang W, Williams DS, Koretsky AP. Measurement of rat brain perfusion by NMR using spin labeling of arterial water: in vivo determination of the degree of spin labeling. *Magn Reson Med*. 1993;29:416–421.
16. Maccotta L, Detre JA, Alsop DC. The efficiency of adiabatic inversion for perfusion imaging by arterial spin labeling. *NMR Biomed*. 1997;10:216–221.
17. Utting JF, Thomas DL, Gadian DG, et al. Velocity-driven adiabatic fast passage for arterial spin labeling: results from a computer model. *Magn Reson Med*. 2003;49:398–401.
18. Gach HM, Kam AW, Reid ED, et al. Quantitative analysis of adiabatic fast passage for steady laminar and turbulent flows. *Magn Reson Med*. 2002;47:709–719.
19. Edelman RR, Siewert B, Darby DG, et al. Qualitative mapping of cerebral blood flow and functional localization with echo-planar MR imaging and signal targeting with alternating radio frequency. *Radiology*. 1994;192:513–520.
20. Kim SG. Quantification of relative cerebral blood flow change by flow-sensitive alternating inversion recovery (FAIR) technique: application to functional mapping. *Magn Reson Med*. 1995;34:293–301.
21. Wolff SD, Balaban RS. Magnetization transfer contrast (MTC) and tissue water proton relaxation in vivo. *Magn Reson Med*. 1989;10:135–144.
22. Henkelman RM, Huang X, Xiang QS, et al. Quantitative interpretation of magnetization transfer. *Magn Reson Med*. 1993;29:759–766.
23. Silva AC, Zhang W, Williams DS, et al. Multi-slice MRI of rat brain perfusion during amphetamine stimulation using arterial spin labeling. *Magn Reson Med*. 1995;33:209–214.
24. Zhang W, Silva AC, Williams DS, et al. NMR measurement of perfusion using arterial spin labeling without saturation of macromolecular spins. *Magn Reson Med*. 1995;33:370–376.
25. Trampel R, Mildner T, Goerke U, et al. Continuous arterial spin labeling using a local magnetic field gradient coil. *Magn Reson Med*. 2002;48:543–546.
26. Zaharchuk G, Ledden PJ, Kwong KK, et al. Multislice perfusion and perfusion territory imaging in humans with separate label and image coils. *Magn Reson Med*. 1999;41:1093–1098.
27. Mildner T, Trampel R, Moller HE, et al. Functional perfusion imaging using continuous arterial spin labeling with separate labeling and imaging coils at 3 T. *Magn Reson Med*. 2003;49:791–795.
28. Alsop DC, Detre JA. Multisection cerebral blood flow MR imaging with continuous arterial spin labeling. *Radiology*. 1998;208:410–416.
29. Naidu S, Kaufmann WE, Abrams MT, et al. Neuroimaging studies in Rett syndrome. *Brain Dev*. 2001;23(suppl 1):62–71.
30. Schwarzbauer C, Morrissey SP, Haase A. Quantitative magnetic resonance imaging of perfusion using magnetic labeling of water proton spins within the detection slice. *Magn Reson Med*. 1996;35:540–546.
31. Calamante F, Williams SR, van Bruggen N, et al. A model for quantification of perfusion in pulsed labelling techniques. *NMR Biomed*. 1996;9:79–83.
32. Kim SG, Tsekos NV. Perfusion imaging by a flow-sensitive alternating inversion recovery (FAIR) technique: application to functional brain imaging. *Magn Reson Med*. 1997;37:425–435.
33. Kao YH, Wan X, MacFall JR. Simultaneous multislice acquisition with arterial-flow tagging (SMART) using echo planar imaging (EPI). *Magn Reson Med*. 1998;39:662–665.
34. Yang Y, Frank JA, Hou L, et al. Multislice imaging of quantitative cerebral perfusion with pulsed arterial spin labeling. *Magn Reson Med*. 1998;39:825–832.
35. Wong EC, Buxton RB, Frank LR. Implementation of quantitative perfusion imaging techniques for functional brain mapping using pulsed arterial spin labeling. *NMR Biomed*. 1997;10:237–249.
36. Yongbi MN, Branch CA, Helpern JA. Perfusion imaging using FOCI RF pulses. *Magn Reson Med*. 1998;40:938–943.
37. Tanabe JL, Yongbi M, Branch C, et al. MR perfusion imaging in human brain using the UNFAIR technique: un-inverted flow-sensitive alternating inversion recovery. *J Magn Reson Imaging*. 1999;9:761–767.
38. Berr SS, Mai VM. Extraslice spin tagging (EST) magnetic resonance imaging for the determination of perfusion. *J Magn Reson Imaging*. 1999;9:146–150.
39. Berr SS, Hagspiel KD, Mai VM, et al. Perfusion of the kidney using extraslice spin tagging (EST) magnetic resonance imaging. *J Magn Reson Imaging*. 1999;10:886–891.
40. Zhou J, Mori S, van Zijl PC. FAIR excluding radiation damping (FAIRER). *Magn Reson Med*. 1998;40:712–719.
41. Zhou J, van Zijl PC. Perfusion imaging using FAIR with a short predelay. *Magn Reson Med*. 1999;41:1099–1107.
42. Mai VM, Berr SS. MR perfusion imaging of pulmonary parenchyma using pulsed arterial spin labeling techniques: FAIRER and FAIR. *J Magn Reson Imaging*. 1999;9:483–487.
43. Mai VM, Hagspiel KD, Christopher JM, et al. Perfusion imaging of the human lung using flow-sensitive alternating inversion recovery with an extra radiofrequency pulse (FAIRER). *Magn Reson Imaging*. 1999;17:355–361.
44. Lai S, Wang J, Jahng GH. FAIR exempting separate T (1) measurement (FAIREST): a novel technique for online quantitative perfusion imaging and multi-contrast fMRI. *NMR Biomed*. 2001;14:507–516.
45. Pell GS, Thomas DL, Lythgoe MF, et al. Implementation of quantitative FAIR perfusion imaging with a short repetition time in time-course studies. *Magn Reson Med*. 1999;41:829–840.
46. Schwarzbauer C, Heinke W. BASE imaging: a new spin labeling technique for measuring absolute perfusion changes. *Magn Reson Med*. 1998;39:717–722.
47. Edelman RR, Chen Q. EPISTAR MRI: multislice mapping of cerebral blood flow. *Magn Reson Med*. 1998;40:800–805.
48. Golay X, Stuber M, Pruessmann KP, et al. Transfer insensitive labeling technique (TILT): application to multislice functional perfusion imaging. *J Magn Reson Imaging*. 1999;9:454–461.
49. Pruessmann KP, Golay X, Stuber M, et al. RF pulse concatenation for spatially selective inversion. *J Magn Reson*. 2000;146:58–65.
50. Jahng GH, Zhu XP, Matson GB, et al. Improved perfusion-weighted MRI by a novel double inversion with proximal labeling of both tagged and control acquisitions. *Magn Reson Med*. 2003;49:307–314.
51. Wong EC, Buxton RB, Frank LR. Quantitative imaging of perfusion using a single subtraction (QUIPSS and QUIPSS II). *Magn Reson Med*. 1998;39:702–708.
52. Wong EC, Buxton RB, Frank LR. A theoretical and experimental comparison of continuous and pulsed arterial spin labeling techniques for quantitative perfusion imaging. *Magn Reson Med*. 1998;40:348–355.
53. Luh WM, Wong EC, Bandettini PA, et al. QUIPSS II with thin-slice TI1 periodic saturation: a method for improving accuracy of quantitative per-


 

fusion imaging using pulsed arterial spin labeling. *Magn Reson Med*. 1999;41:1246–1254.
54. Luh WM, Wong EC, Bandettini PA, et al. Comparison of simultaneously measured perfusion and BOLD signal increases during brain activation with T(1)-based tissue identification. *Magn Reson Med*. 2000;44:137–143.
55. Wong EC, Luh WM, Liu TT. Turbo ASL: arterial spin labeling with higher SNR and temporal resolution. *Magn Reson Med*. 2000;44:511–515.
56. Silva AC, Kim SG. Pseudo-continuous arterial spin labeling technique for measuring CBF dynamics with high temporal resolution. *Magn Reson Med*. 1999;42:425–429.
57. Barbier EL, Silva AC, Kim HJ, et al. Perfusion analysis using dynamic arterial spin labeling (DASL). *Magn Reson Med*. 1999;41:299–308.
58. Barbier EL, Silva AC, Kim SG, et al. Perfusion imaging using dynamic arterial spin labeling (DASL). *Magn Reson Med*. 2001;45:1021–1029.
59. Mani S, Pauly J, Conolly S, et al. Background suppression with multiple inversion recovery nulling: applications to projective angiography. *Magn Reson Med*. 1997;37:898–905.
60. Ye FQ, Frank JA, Weinberger DR, et al. Noise reduction in 3D perfusion imaging by attenuating the static signal in arterial spin tagging (ASSIST). *Magn Reson Med*. 2000;44:92–100.
61. Blamire AM, Styles P. Spin echo entrapped perfusion image (SEEPAGE): a nonsubtraction method for direct imaging of perfusion. *Magn Reson Med*. 2000;43:701–704.
62. Duyn JH, Tan CX, van Gelderen P, et al. High-sensitivity single-shot perfusion-weighted fMRI. *Magn Reson Med*. 2001;46:88–94.
63. Buxton RB, Frank LR, Wong EC, et al. A general kinetic model for quantitative perfusion imaging with arterial spin labeling. *Magn Reson Med*. 1998;40:383–396.
64. Alsop DC, Detre JA. Reduced transit-time sensitivity in noninvasive magnetic resonance imaging of human cerebral blood flow. *J Cereb Blood Flow Metab*. 1996;16:1236–1249.
65. Chesler DA, Kwong KK. An intuitive guide to the T1 based perfusion model. *Int J Imaging Syst Technol*. 1995;6:171–174.</jrn>
66. Pekar J, Jezzard P, Roberts DA, et al. Perfusion imaging with compensation for asymmetric magnetization transfer effects. *Magn Reson Med*. 1996;35:70–79.
67. McLaughlin AC, Ye FQ, Pekar JJ, et al. Effect of magnetization transfer on the measurement of cerebral blood flow using steady-state arterial spin tagging approaches: a theoretical investigation. *Magn Reson Med*. 1997;37:501–510.
68. Silva AC, Zhang W, Williams DS, et al. Estimation of water extraction fractions in rat brain using magnetic resonance measurement of perfusion with arterial spin labeling. *Magn Reson Med*. 1997;37:58–68.
69. Parkes LM, Tofts PS. Improved accuracy of human cerebral blood perfusion measurements using arterial spin labeling: accounting for capillary water permeability. *Magn Reson Med*. 2002;48:27–41.
70. Zhou J, Wilson DA, Ulatowski JA, et al. Two-compartment exchange model for perfusion quantification using arterial spin tagging. *J Cereb Blood Flow Metab*. 2001;21:440–455.
71. St. Lawrence KS, Frank JA, McLaughlin AC. Effect of restricted water exchange on cerebral blood flow values calculated with arterial spin tagging: a theoretical investigation. *Magn Reson Med*. 2000;44:440–449.
72. Ewing JR, Cao Y, Fenstermacher J. Single-coil arterial spin-tagging for estimating cerebral blood flow as viewed from the capillary: relative contributions of intra- and extravascular signal. *Magn Reson Med*. 2001; 46:465–475.
73. Yongbi MN, Tan CX, Frank JA, et al. A protocol for assessing subtraction errors of arterial spin-tagging perfusion techniques in human brain. *Magn Reson Med*. 2000;43:896–900.
74. Oguz KK, Golay X, Pizzini FB, et al. Sickle cell disease: continuous arterial spin-labeling perfusion MR imaging in children. *Radiology*. 2003;227:567–574.
75. Lei H, Peeling J. A strategy to optimize the signal-to-noise ratio in one-coil arterial spin tagging perfusion imaging. *Magn Reson Med*. 1999;41: 563–568.
76. Li TQ, Moseley ME, Glover G. A FAIR study of motor cortex activation under normo- and hypercapnia induced by breath challenge. *Neuroimage*. 1999;10:562–569.
77. Yang Y, Gu H, Zhan W, et al. Simultaneous perfusion and BOLD imaging using reverse spiral scanning at 3T: characterization of functional contrast and susceptibility artifacts. *Magn Reson Med*. 2002;48:278–289.
78. Zhang W. A quantitative analysis of alternated line scanning in k space and its application in MRI of regional tissue perfusion by arterial spin labeling. *J Magn Reson B*. 1995;107:165–171.
79. Branch CA, Hernandez L, Yongbi M, et al. Rapid and continuous monitoring of cerebral perfusion by magnetic resonance line scan assessment with arterial spin tagging. *NMR Biomed*. 1999;12:15–25.
80. Chen Q, Siewert B, Bly BM, et al. STAR-HASTE: perfusion imaging without magnetic susceptibility artifact. *Magn Reson Med*. 1997;38: 404–408.
81. Crelier GR, Hoge RD, Munger P, et al. Perfusion-based functional magnetic resonance imaging with single-shot RARE and GRASE acquisitions. *Magn Reson Med*. 1999;41:132–136.
82. Liu HL, Kochunov P, Hou J, et al. Perfusion-weighted imaging of interictal hypoperfusion in temporal lobe epilepsy using FAIR-HASTE: comparison with H(2)(15)O PET measurements. *Magn Reson Med*. 2001;45:431–435.
83. Prasad PV, Kim D, Kaiser AM, et al. Noninvasive comprehensive characterization of renal artery stenosis by combination of STAR angiography and EPISTAR perfusion imaging. *Magn Reson Med*. 1997;38:776–787.
84. Frank LR, Wong EC, Haseler LJ, et al. Dynamic imaging of perfusion in human skeletal muscle during exercise with arterial spin labeling. *Magn Reson Med*. 1999;42:258–267.
85. Raynaud JS, Duteil S, Vaughan JT, et al. Determination of skeletal muscle perfusion using arterial spin labeling NMRI: validation by comparison with venous occlusion plethysmography. *Magn Reson Med*. 2001;46:305–311.
86. Richardson RS, Haseler LJ, Nygren AT, et al. Local perfusion and metabolic demand during exercise: a noninvasive MRI method of assessment. *J Appl Physiol*. 2001;91:1845–1853.
87. Reeder SB, Atalay MK, McVeigh ER, et al. Quantitative cardiac perfusion: a noninvasive spin-labeling method that exploits coronary vessel geometry. *Radiology*. 1996;200:177–184.
88. Belle V, Kahler E, Waller C, et al. In vivo quantitative mapping of cardiac perfusion in rats using a noninvasive MR spin-labeling method. *J Magn Reson Imaging*. 1998;8:1240–1245.
89. Reeder SB, Holmes AA, McVeigh ER, et al. Simultaneous noninvasive determination of regional myocardial perfusion and oxygen content in rabbits: toward direct measurement of myocardial oxygen consumption at MR imaging. *Radiology*. 1999;212:739–747.
90. Waller C, Kahler E, Hiller KH, et al. Myocardial perfusion and intracapillary blood volume in rats at rest and with coronary dilatation: MR imaging in vivo with use of a spin-labeling technique. *Radiology*. 2000; 215:189–197.
91. Waller C, Hiller KH, Voll S, et al. Myocardial perfusion imaging using a non-contrast agent MR imaging technique. *Int J Cardiovasc Imaging*. 2001;17:123–132.
92. Streif JU, Hiller KH, Waller C, et al. In vivo assessment of absolute perfusion in the murine skeletal muscle with spin labeling MRI: magnetic resonance imaging. *J Magn Reson Imaging*. 2003;17:147–152.
93. Marro KI, Kushmerick MJ. Skeletal muscle perfusion measurements using adiabatic inversion of arterial water. *Magn Reson Med*. 1997;38: 40–47.
94. Toussaint JF, Kwong KK. M'Kparu F, et al. Interrelationship of oxidative metabolism and local perfusion demonstrated by NMR in human skeletal muscle. *J Appl Physiol*. 1996;81:2221–2228.
95. Roberts DA, Gefter WB, Hirsch JA, et al. Pulmonary perfusion: respiratory-triggered three-dimensional MR imaging with arterial spin tagging—preliminary results in healthy volunteers. *Radiology*. 1999;212: 890–895.
96. Hatabu H, Tadamura E, Prasad PV, et al. Noninvasive pulmonary perfusion imaging by STAR-HASTE sequence. *Magn Reson Med*. 2000; 44:808–812.
97. Mai VM, Chen Q, Bankier AA, et al. Effect of lung inflation on arterial spin labeling signal in MR perfusion imaging of human lung. *J Magn Reson Imaging*. 2001;13:954–959.

 

98. Mai VM, Bankier AA, Prasad PV, et al. MR ventilation-perfusion imaging of human lung using oxygen-enhanced and arterial spin labeling techniques. *J Magn Reson Imaging*. 2001;14:574–579.
99. Wang JJ, Hendrich KS, Jackson EK, et al. Perfusion quantitation in transplanted rat kidney by MRI with arterial spin labeling. *Kidney Int*. 1998;53:1783–1791.
100. Tempel C, Neeman M. Spatial and temporal modulation of perfusion in the rat ovary measured by arterial spin labeling MRI. *J Magn Reson Imaging*. 1999;9:794–803.
101. Tempel C, Neeman M. Perfusion of the rat ovary: application of pulsed arterial spin labeling MRI. *Magn Reson Med*. 1999;41:113–123.
102. Karger N, Biederer J, Lusse S, et al. Quantitation of renal perfusion using arterial spin labeling with FAIR-UFLARE. *Magn Reson Imaging*. 2000; 18:641–647.
103. Ye FQ, Mattay VS, Jezzard P, et al. Correction for vascular artifacts in cerebral blood flow values measured by using arterial spin tagging techniques. *Magn Reson Med*. 1997;37:226–235.
104. Pell GS, Lewis DP, Branch CA. Pulsed arterial spin labeling using TurboFLASH with suppression of intravascular signal. *Magn Reson Med*. 2003;49:341–350.
105. Wang J, Alsop DC, Song HK, et al. Arterial transit time imaging with flow encoding arterial spin tagging (FEAST). *Magn Reson Med*. 2003; 50:599–607.
106. Frank LR, Wong EC, Buxton RB. Slice profile effects in adiabatic inversion: application to multislice perfusion imaging. *Magn Reson Med*. 1997;38:558–564.
107. Schepers J, Garwood M, van der Sanden B, et al. Improved subtraction by adiabatic FAIR perfusion imaging. *Magn Reson Med*. 2002;47:330–336.
108. Zhan W, Gu H, Silbersweig DA, et al. Inversion profiles of adiabatic inversion pulses for flowing spins: the effects on labeling efficiency and labeling accuracy in perfusion imaging with pulsed arterial spin-labeling. *Magn Reson Imaging*. 2002;20:487–494.
109. Keilholz-George SD, Knight-Scott J, Berr SS. Theoretical analysis of the effect of imperfect slice profiles on tagging schemes for pulsed arterial spin labeling MRI. *Magn Reson Med*. 2001;46:141–148.
110. Yongbi MN, Yang Y, Frank JA, et al. Multislice perfusion imaging in human brain using the C-FOCI inversion pulse: comparison with hyperbolic secant. *Magn Reson Med*. 1999;42:1098–1105.
111. Shinnar M, Leigh JS. The application of spinors to pulse synthesis and analysis. *Magn Reson Med*. 1989;12:93–98.
112. Kwong KK, Belliveau JW, Chesler DA, et al. Dynamic magnetic resonance imaging of human brain activity during primary sensory stimulation. *Proc Natl Acad Sci USA*. 1992;89:5675–5679.
113. Bandettini PA, Wong EC, Hinks RS, et al. Time course EPI of human brain function during task activation. *Magn Reson Med*. 1992;25:390–397.
114. Ogawa S, Lee TM, Kay AR, et al. Brain magnetic resonance imaging with contrast dependent on blood oxygenation. *Proc Natl Acad Sci USA*. 1990;87:9868–9872.
115. Kim SG, Tsekos NV, Ashe J. Multi-slice perfusion-based functional MRI using the FAIR technique: comparison of CBF and BOLD effects. *NMR Biomed*. 1997;10:191–196.
116. Buxton RB, Wong EC, Frank LR. Dynamics of blood flow and oxygenation changes during brain activation: the balloon model. *Magn Reson Med*. 1998;39:855–864.
117. Ye FQ, Smith AM, Yang Y, et al. Quantitation of regional cerebral blood flow increases during motor activation: a steady-state arterial spin tagging study. *Neuroimage*. 1997;6:104–112.
118. Ye FQ, Yang Y, Duyn J, et al. Quantitation of regional cerebral blood flow increases during motor activation: a multislice, steady-state, arterial spin tagging study. *Magn Reson Med*. 1999;42:404–407.
119. Schulte AC, Speck O, Oesterle C, et al. Separation and quantification of perfusion and BOLD effects by simultaneous acquisition of functional I(0)- and T2(*)-parameter maps. *Magn Reson Med*. 2001;45:811–816.
120. Zhu XH, Kim SG, Andersen P, et al. Simultaneous oxygenation and perfusion imaging study of functional activity in primary visual cortex at different visual stimulation frequency: quantitative correlation between BOLD and CBF changes. *Magn Reson Med*. 1998;40:703–711.
121. Talagala SL, Noll DC. Functional MRI using steady-state arterial water labeling. *Magn Reson Med*. 1998;39:179–183.
122. Darby DG, Nobre AC, Thangaraj V, et al. Cortical activation in the human brain during lateral saccades using EPISTAR functional magnetic resonance imaging. *Neuroimage*. 1996;3:53–62.
123. Ye FQ, Smith AM, Mattay VS, et al. Quantitation of regional cerebral blood flow increases in prefrontal cortex during a working memory task: a steady-state arterial spin-tagging study. *Neuroimage*. 1998;8:44–49.
124. Aguirre GK, Detre JA, Zarahn E, et al. Experimental design and the relative sensitivity of BOLD and perfusion fMRI. *Neuroimage*. 2002;15: 488–500.
125. Detre JA, Wang J. Technical aspects and utility of fMRI using BOLD and ASL. *Clin Neurophysiol*. 2002;113:621–634.
126. Wang J, Aguirre GK, Kimberg DY, et al. Arterial spin labeling perfusion fMRI with very low task frequency. *Magn Reson Med*. 2003;49:796–802.
127. Kim SG, Ugurbil K. Comparison of blood oxygenation and cerebral blood flow effects in fMRI: estimation of relative oxygen consumption change. *Magn Reson Med*. 1997;38:59–65.
128. Preibisch C, Haase A. Perfusion imaging using spin-labeling methods: contrast-to-noise comparison in functional MRI applications. *Magn Reson Med*. 2001;46:172–182.
129. Tsekos NV, Zhang F, Merkle H, et al. Quantitative measurements of cerebral blood flow in rats using the FAIR technique: correlation with previous iodoantipyrine autoradiographic studies. *Magn Reson Med*. 1998;39:564–573.
130. Duong TQ, Kim SG. In vivo MR measurements of regional arterial and venous blood volume fractions in intact rat brain. *Magn Reson Med*. 2000;43:393–402.
131. Duong TQ, Kim DS, Ugurbil K, et al. Localized cerebral blood flow response at submillimeter columnar resolution. *Proc Natl Acad Sci USA*. 2001;98:10904–10909.
132. Lee SP, Silva AC, Kim SG. Comparison of diffusion-weighted high-resolution CBF and spin-echo BOLD fMRI at 9.4 T. *Magn Reson Med*. 2002;47:736–741.
133. Liu HL, Pu Y, Nickerson LD, et al. Comparison of the temporal response in perfusion and BOLD-based event-related functional MRI. *Magn Reson Med*. 2000;43:768–772.
134. Liu HL, Gao JH. Perfusion-based event-related functional MRI. *Magn Reson Med*. 1999;42:1011–1013.
135. Yang Y, Engelien W, Pan H, et al. A CBF-based event-related brain activation paradigm: characterization of impulse-response function and comparison to BOLD. *Neuroimage*. 2000;12:287–297.
136. Zhou J, van Zijl PC. Effect of transit times on quantification of cerebral blood flow by the FAIR T(1)-difference approach. *Magn Reson Med*. 1999;42:890–894.
137. Gonzalez-At JB, Alsop DC, Detre JA. Cerebral perfusion and arterial transit time changes during task activation determined with continuous arterial spin labeling. *Magn Reson Med*. 2000;43:739–746.
138. Yang Y, Engelien W, Xu S, et al. Transit time, trailing time, and cerebral blood flow during brain activation: measurement using multislice, pulsed spin-labeling perfusion imaging. *Magn Reson Med*. 2000;44: 680–685.
139. Gunther M, Bock M, Schad LR. Arterial spin labeling in combination with a look-locker sampling strategy: inflow turbo-sampling EPI-FAIR (ITS-FAIR). *Magn Reson Med*. 2001;46:974–984.
140. Hendrikse J, Lu H, van der Grond J, et al. Measurements of cerebral perfusion and arterial hemodynamics during visual stimulation using TURBO-TILT. *Magn Reson Med*. 2003;50:429–433.
141. Wang J, Aguirre GK, Kimberg DY, et al. Empirical analyses of null-hypothesis perfusion FMRI data at 1.5 and 4 T. *Neuroimage*. 2003;19: 1449–1462.
142. Davis TL, Kwong KK, Weisskoff RM, et al. Calibrated functional MRI: mapping the dynamics of oxidative metabolism. *Proc Natl Acad Sci USA*. 1998;95:1834–1839.
143. Kim SG, Rostrup E, Larsson HB, et al. Determination of relative CMRO2 from CBF and BOLD changes: significant increase of oxygen consumption rate during visual stimulation. *Magn Reson Med*. 1999;41: 1152–1161.
144. Hoge RD, Atkinson J, Gill B, et al. Linear coupling between cerebral


 

blood flow and oxygen consumption in activated human cortex. *Proc Natl Acad Sci USA*. 1999;96:9403–9408.
145. Hoge RD, Atkinson J, Gill B, et al. Stimulus-dependent BOLD and perfusion dynamics in human V1. *Neuroimage*. 1999;9:573–585.
146. Duong TQ, Iadecola C, Kim SG. Effect of hyperoxia, hypercapnia, and hypoxia on cerebral interstitial oxygen tension and cerebral blood flow. *Magn Reson Med*. 2001;45:61–70.
147. Silva AC, Lee SP, Yang G, et al. Simultaneous blood oxygenation level-dependent and cerebral blood flow functional magnetic resonance imaging during forepaw stimulation in the rat. *J Cereb Blood Flow Metab*. 1999;19:871–879.
148. Silva AC, Lee SP, Iadecola C, et al. Early temporal characteristics of cerebral blood flow and deoxyhemoglobin changes during somatosensory stimulation. *J Cereb Blood Flow Metab*. 2000;20:201–206.
149. Ernst T, Hennig J. Observation of a fast response in functional MR. *Magn Reson Med*. 1994;32:146–149.
150. Kim SG, Duong TQ. Mapping cortical columnar structures using fMRI. *Physiol Behav*. 2002;77:641–644.
151. Miller KL, Luh WM, Liu TT, et al. Nonlinear temporal dynamics of the cerebral blood flow response. *Hum Brain Mapp*. 2001;13:1–12.
152. Salmeron BJ, Stein EA. Pharmacological applications of magnetic resonance imaging. *Psychopharmacol Bull*. 2002;36:102–129.
153. Robertson CL, Hendrich KS, Kochanek PM, et al. Assessment of 2-chloroadenosine treatment after experimental traumatic brain injury in the rat using arterial spin-labeled MRI: a preliminary report. *Acta Neurochir Suppl*. 2000;76:187–189.
154. Kochanek PM, Hendrich KS, Robertson CL, et al. Assessment of the effect of 2-chloroadenosine in normal rat brain using spin-labeled MRI measurement of perfusion. *Magn Reson Med*. 2001;45:924–929.
155. Brown GG, Eyler Zorrilla LT, Georgy B, et al. BOLD and perfusion response to finger-thumb apposition after acetazolamide administration: differential relationship to global perfusion. *J Cereb Blood Flow Metab*. 2003;23:829–837.
156. Detre JA, Samuels OB, Alsop DC, et al. Noninvasive magnetic resonance imaging evaluation of cerebral blood flow with acetazolamide challenge in patients with cerebrovascular stenosis. *J Magn Reson Imaging*. 1999;10:870–875.
157. St. Lawrence KS, Ye FQ, Lewis BK, et al. Effects of indomethacin on cerebral blood flow at rest and during hypercapnia: an arterial spin tagging study in humans. *J Magn Reson Imaging*. 2002;15:628–635.
158. St. Lawrence KS, Ye FQ, Lewis BK, et al. Measuring the effects of indomethacin on changes in cerebral oxidative metabolism and cerebral blood flow during sensorimotor activation. *Magn Reson Med*. 2003;50:99–106.
159. Sicard K, Shen Q, Brevard ME, et al. Regional cerebral blood flow and BOLD responses in conscious and anesthetized rats under basal and hypercapnic conditions: implications for functional MRI studies. *J Cereb Blood Flow Metab*. 2003;23:472–481.
160. Born AP, Rostrup E, Miranda MJ, et al. Visual cortex reactivity in sedated children examined with perfusion MRI (FAIR). *Magn Reson Imaging*. 2002;20:199–205.
161. Ewing JR, Wei L, Knight RA, et al. Direct comparison of local cerebral blood flow rates measured by MRI arterial spin-tagging and quantitative autoradiography in a rat model of experimental cerebral ischemia. *J Cereb Blood Flow Metab*. 2003;23:198–209.
162. Pell GS, King MD, Proctor E, et al. Comparative study of the FAIR technique of perfusion quantification with the hydrogen clearance method. *J Cereb Blood Flow Metab*. 2003;23:689–699.
163. Floyd TF, Ratcliffe SJ, Wang J, et al. Precision of the CASL-perfusion MRI technique for the measurement of cerebral blood flow in whole brain and vascular territories. *J Magn Reson Imaging*. 2003;18:649–655.
164. Wang J, Licht DJ, Jahng GH, et al. Pediatric perfusion imaging using pulsed arterial spin labeling. *J Magn Reson Imaging*. 2003;18:404–413.
165. Lia TQ, Guang Chen Z, Ostergaard L, et al. Quantification of cerebral blood flow by bolus tracking and artery spin tagging methods. *Magn Reson Imaging*. 2000;18:503–512.
166. Lia TQ, Haefelin TN, Chan B, et al. Assessment of hemodynamic response during focal neural activity in human using bolus tracking, arterial spin labeling and BOLD techniques. *Neuroimage*. 2000;12:442–451.
167. Ye FQ, Berman KF, Ellmore T, et al. H(2)(15)O PET validation of steady-state arterial spin tagging cerebral blood flow measurements in humans. *Magn Reson Med*. 2000;44:450–456.
168. Liachenko S, Tang P, Hamilton RL, et al. Regional dependence of cerebral reperfusion after circulatory arrest in rats. *J Cereb Blood Flow Metab*. 2001;21:1320–1329.
169. Liachenko S, Tang P, Xu Y. Deferoxamine improves early postresuscitation reperfusion after prolonged cardiac arrest in rats. *J Cereb Blood Flow Metab*. 2003;23:574–581.
170. Xu Y, Liachenko S, Tang P. Dependence of early cerebral reperfusion and long-term outcome on resuscitation efficiency after cardiac arrest in rats. *Stroke*. 2002;33:837–843.
171. Krep H, Bottiger BW, Bock C, et al. Time course of circulatory and metabolic recovery of cat brain after cardiac arrest assessed by perfusion- and diffusion-weighted imaging and MR-spectroscopy. *Resuscitation*. 2003;58:337–348.
172. Schoning M, Niemann G, Hartig B. Transcranial color duplex sonography of basal cerebral arteries: reference data of flow velocities from childhood to adulthood. *Neuropediatrics*. 1996;27:249–255.
173. Schoning M, Hartig B. Age dependence of total cerebral blood flow volume from childhood to adulthood. *J Cereb Blood Flow Metab*. 1996;16:827–833.
174. Calamante F, Lythgoe MF, Pell GS, et al. Early changes in water diffusion, perfusion, T1, and T2 during focal cerebral ischemia in the rat studied at 8.5 T. *Magn Reson Med*. 1999;41:479–485.
175. Zaharchuk G, Mandeville JB, Bogdanov AA Jr, et al. Cerebrovascular dynamics of autoregulation and hypoperfusion: an MRI study of CBF and changes in total and microvascular cerebral blood volume during hemorrhagic hypotension. *Stroke*. 1999;30:2197–2204; discussion 2204–2195.
176. Lythgoe MF, Thomas DL, Calamante F, et al. Acute changes in MRI diffusion, perfusion, T(1), and T(2) in a rat model of oligemia produced by partial occlusion of the middle cerebral artery. *Magn Reson Med*. 2000;44:706–712.
177. Chalela JA, Alsop DC, Gonzalez-Atavales JB, et al. Magnetic resonance perfusion imaging in acute ischemic stroke using continuous arterial spin labeling. *Stroke*. 2000;31:680–687.
178. Detre JA, Alsop DC. Perfusion magnetic resonance imaging with continuous arterial spin labeling: methods and clinical applications in the central nervous system. *Eur J Radiol*. 1999;30:115–124.
179. Tsuchiya K, Katase S, Hachiya J, et al. Cerebral perfusion MRI with arterial spin labeling technique at 0.5 Tesla. *J Comput Assist Tomogr*. 2000;24:124–127.
180. Siewert B, Schlaug G, Edelman RR, et al. Comparison of EPISTAR and T2*-weighted gadolinium-enhanced perfusion imaging in patients with acute cerebral ischemia. *Neurology*. 1997;48:673–679.
181. Yen YF, Field AS, Martin EM, et al. Test-retest reproducibility of quantitative CBF measurements using FAIR perfusion MRI and acetazolamide challenge. *Magn Reson Med*. 2002;47:921–928.
182. Gaa J, Warach S, Wen P, et al. Noninvasive perfusion imaging of human brain tumors with EPISTAR. *Eur Radiol*. 1996;6:518–522.
183. Silva AC, Kim SG, Garwood M. Imaging blood flow in brain tumors using arterial spin labeling. *Magn Reson Med*. 2000;44:169–173.
184. Warmuth C, Gunther M, Zimmer C. Quantification of blood flow in brain tumors: comparison of arterial spin labeling and dynamic susceptibility-weighted contrast-enhanced MR imaging. *Radiology*. 2003;228:523–532.
185. Nobauer-Huhmann IM, Ba-Ssalamah A, Mlynarik V, et al. Magnetic resonance imaging contrast enhancement of brain tumors at 3 tesla versus 1.5 tesla. *Invest Radiol*. 2002;37:114–119.
186. Ba-Ssalamah A, Nobauer-Huhmann IM, Pinker K, et al. Effect of contrast dose and field strength in the magnetic resonance detection of brain metastases. *Invest Radiol*. 2003;38:415–422.
187. Brown SL, Ewing JR, Kolozsvary A, et al. Magnetic resonance imaging of perfusion in rat cerebral 9L tumor after nicotinamide administration. *Int J Radiat Oncol Biol Phys*. 1999;43:627–633.
188. Schmitt P, Kotas M, Tobermann A, et al. Quantitative tissue perfusion measurements in head and neck carcinoma patients before and during radiation therapy with a non-invasive MR imaging spin-labeling technique. *Radiother Oncol*. 2003;67:27–34.

 

189. Alsop DC, Detre JA, Grossman M. Assessment of cerebral blood flow in Alzheimer's disease by spin-labeled magnetic resonance imaging. *Ann Neurol*. 2000;47:93–100.
190. Sandson TA, O'Connor M, Sperling RA, et al. Noninvasive perfusion MRI in Alzheimer's disease: a preliminary report. *Neurology*. 1996;47: 1339–1342.
191. Wolf RL, Alsop DC, Levy-Reis I, et al. Detection of mesial temporal lobe hypoperfusion in patients with temporal lobe epilepsy by use of arterial spin labeled perfusion MR imaging. *AJNR Am J Neuroradiol*. 2001;22:1334–1341.
192. Doraiswamy PM, MacFall J, Krishnan KR, et al. Magnetic resonance assessment of cerebral perfusion in depressed cardiac patients: preliminary findings. *Am J Psychiatry*. 1999;156:1641–1643.
193. Chalela JA, Kasner SE, McGarvey M, et al. Continuous arterial spin labeling perfusion magnetic resonance imaging findings in postpartum vasculopathy. *J Neuroimaging*. 2001;11:444–446.
194. Golay X, Eichler F, Barker PB, et al. Cerebral blood flow in Rett syndrome: evaluation with continuous arterial spin labeling. Glasgow. *Proceedings of the 9th ISMRM*. 2001:1575.
195. Moore DF, Ye F, Schiffmann R, et al. Increased signal intensity in the pulvinar on T1-weighted images: a pathognomonic MR imaging sign of Fabry disease. *AJNR Am J Neuroradiol*. 2003;24:1096–1101.
196. Forbes ML, Hendrich KS, Kochanek PM, et al. Assessment of cerebral blood flow and $CO_2$ reactivity after controlled cortical impact by perfusion magnetic resonance imaging using arterial spin-labeling in rats. *J Cereb Blood Flow Metab*. 1997;17:865–874.
197. Mai VM, Hagspiel KD, Altes T, et al. Detection of regional pulmonary perfusion deficit of the occluded lung using arterial spin labeling in magnetic resonance imaging. *J Magn Reson Imaging*. 2000;11:97–102.
198. Keilholz SD, Knight-Scott J, Christopher JM, et al. Gravity-dependent perfusion of the lung demonstrated with the FAIRER arterial spin tagging method. *Magn Reson Imaging*. 2001;19:929–935.
199. Roberts DA, Rizi RR, Lipson DA, et al. Dynamic observation of pulmonary perfusion using continuous arterial spin-labeling in a pig model. *J Magn Reson Imaging*. 2001;14:175–180.
200. Uematsu H, Levin DL, Hatabu H. Quantification of pulmonary perfusion with MR imaging: recent advances. *Eur J Radiol*. 2001;37:155–163.
201. Keilholz SD, Mai VM, Berr SS, et al. Comparison of first-pass Gd-DOTA and FAIRER MR perfusion imaging in a rabbit model of pulmonary embolism. *J Magn Reson Imaging*. 2002;16:168–171.
202. Lipson DA, Roberts DA, Hansen-Flaschen J, et al. Pulmonary ventilation and perfusion scanning using hyperpolarized helium-3 MRI and arterial spin tagging in healthy normal subjects and in pulmonary embolism and orthotopic lung transplant patients. *Magn Reson Med*. 2002;47: 1073–1076.
203. Mai VM, Liu B, Polzin JA, et al. Ventilation-perfusion ratio of signal intensity in human lung using oxygen-enhanced and arterial spin labeling techniques. *Magn Reson Med*. 2002;48:341–350.
204. Rizi RR, Lipson DA, Dimitrov IE, et al. Operating characteristics of hyperpolarized 3He and arterial spin tagging in MR imaging of ventilation and perfusion in healthy subjects. *Acad Radiol*. 2003;10:502–508.
205. Uematsu H, Ohno Y, Hatabu H. Recent advances in magnetic resonance perfusion imaging of the lung. *Top Magn Reson Imaging*. 2003;14:245–251.
206. Wang T, Schultz G, Hebestreit H, et al. Quantitative perfusion mapping of the human lung using 1H spin labeling. *J Magn Reson Imaging*. 2003; 18:260–265.
207. Hiller KH, Waller C, Voll S, et al. Combined high-speed NMR imaging of perfusion and microscopic coronary conductance vessels in the isolated rat heart. *Microvasc Res*. 2001;62:327–334.
208. Roberts DA, Detre JA, Bolinger L, et al. Renal perfusion in humans: MR imaging with spin tagging of arterial water. *Radiology*. 1995;196:281–286.
209. Zhu DC, Buonocore MH. Breast tissue differentiation using arterial spin tagging. *Magn Reson Med*. 2003;50:966–975.
210. Hagspiel KD, Matsumoto AH, Berr SS. Uterine fibroid embolization: assessment of treatment response using perfusion-weighted extraslice spin tagging (EST) magnetic resonance imaging. *J Magn Reson Imaging*. 2001;13:982–986.
211. Wacker CM, Fidler F, Dueren C, et al. Quantitative assessment of myocardial perfusion with a spin-labeling technique: preliminary results in patients with coronary artery disease. *J Magn Reson Imaging*. 2003;18: 555–560.
212. Bernstein MA, Huston J 3rd, Lin C, et al. High-resolution intracranial and cervical MRA at 3.0T: technical considerations and initial experience. *Magn Reson Med*. 2001;46:955–962.
213. Gati JS, Menon RS, Ugurbil K, et al. Experimental determination of the BOLD field strength dependence in vessels and tissue. *Magn Reson Med*. 1997;38:296–302.
214. Barker PB, Hearshen DO, Boska MD. Single-voxel proton MRS of the human brain at 1.5T and 3.0T. *Magn Reson Med*. 2001;45:765–769.
215. Wansapura JP, Holland SK, Dunn RS, et al. NMR relaxation times in the human brain at 3.0 tesla. *J Magn Reson Imaging*. 1999;9:531–538.
216. Yongbi MN, Fera F, Yang Y, et al. Pulsed arterial spin labeling: comparison of multisection baseline and functional MR imaging perfusion signal at 1.5 and 3.0 T: initial results in six subjects. *Radiology*. 2002; 222:569–575.
217. Wang J, Alsop DC, Li L, et al. Comparison of quantitative perfusion imaging using arterial spin labeling at 1.5 and 4.0 Tesla. *Magn Reson Med*. 2002;48:242–254.
218. Lu H, Golay X, van Zijl PC. Intervoxel heterogeneity of event-related functional magnetic resonance imaging responses as a function of T(1) weighting. *Neuroimage*. 2002;17:943–955.
219. Lu H, Clingman C, Golay X, et al. What is the longitudinal relaxation time (T1) of blood at 3.0 Tesla? Toronto. *Proceedings of the 11th ISMRM*. 2003:669.
220. Franke C, van Dorsten FA, Olah L, et al. Arterial spin tagging perfusion imaging of rat brain: dependency on magnetic field strength. *Magn Reson Imaging*. 2000;18:1109–1113.
221. Weber MA, Gunther M, Lichy MP, et al. Comparison of arterial spin-labeling techniques and dynamic susceptibility-weighted contrast-enhanced MRI in perfusion imaging of normal brain tissue. *Invest Radiol*. 2003;38:712–718.
222. Look DC, Locker DR. Time saving in measurement of NMR and EPR relaxation times. *Rev Sci Instrum*. 1970;41:250–251.
223. Edelman RR, Mattle HP, O'Reilly GV, et al. Magnetic resonance imaging of flow dynamics in the circle of Willis. *Stroke*. 1990;21:56–65.
224. Eastwood JD, Holder CA, Hudgins PA, et al. Magnetic resonance imaging with lateralized arterial spin labeling. *Magn Reson Imaging*. 2002; 20:583–586.
225. Davies NP, Jezzard P. Selective arterial spin labeling (SASL): perfusion territory mapping of selected feeding arteries tagged using two-dimensional radiofrequency pulses. *Magn Reson Med*. 2003;49:1133–1142.
226. Hendrikse J, van der Grond J, Lu H, et al. Flow territory mapping of the cerebral arteries with regional Perfusion MRI (RPI). *Stroke*. 2004; (in press).
227. Duhamel G, de Bazelaire C, Alsop DC. Evaluation of systematic quantification errors in velocity-selective arterial spin labeling of the brain. *Magn Reson Med*. 2003;50:145–153.
228. Norris DG, Schwarzbauer C. Velocity selective radiofrequency pulse trains. *J Magn Reson*. 1999;137:231–236.
229. Wong EC, Liu TT, Sidaros K, et al. Velocity selective arterial spin labeling, Honolulu. *Proceedings of the 10th ISMRM*. 2002:621.
230. Guilfoyle DN, Gibbs P, Ordidge RJ, et al. Real-time flow measurements using echo-planar imaging. *Magn Reson Med*. 1991;18:1–8.


 